Earth Surf. Dynam. Discuss., https://doi.org/10.5194/esurf-2017-47
Manuscript under review for journal Earth Surf. Dynam.
Discussion started: 16 August 2017

Where is Late Cenozoic climate change most likely to impact denudation?

Sebastian G. Mutz[1], Todd A. Ehlers[1], Martin Werner[2], Gerrit Lohmann[2], Christian Stepanek[2], Jingmin Li[3]

[1] Department of Geosciences, University Tübingen, D-72074 Tübingen, Germany

[2] Department of Paleoclimate Dynamics, Alfred Wegener Institute, Helmholtz Centre for Polar and Marine Research, D-27570 Bremerhaven, Germany

[3] Institute for Geography and Geology, University of Würzburg, Würzburg, D-97074 Germany

Correspondence to: Sebastian G. Mutz (sebastian.mutz@uni-tuebingen.de)

Abstract

The denudation history of active orogens is often interpreted in the context of modern climate and vegetation gradients. Here we address the validity of this approach and ask the question: what are the spatial and temporal variations in paleo-climate for a latitudinally diverse range of active orogens? We do this using high-resolution (T159, ca. 80 x 80 km at the equator) paleo-climate simulations from the ECHAM5 global Atmospheric General Circulation Model and a statistical cluster analysis of climate over different orogens (Andes, Himalaya, SE Alaska, Pacific NW USA). Time periods and boundary conditions considered include the Pliocene (PLIO, ~3 Ma), the Last Glacial Maximum (LGM, ~21 ka), Mid Holocene (MH, ~6 ka) and Pre-Industrial (PI, reference year 1850). The regional simulated climates of each orogen are described by means of cluster analyses based on the variability of precipitation, 2m air temperature, the intra-annual amplitude of these values, and monsoonal wind speeds where appropriate. Results indicate the largest differences to the PI climate are observed for the LGM and PLIO climates in the form of widespread cooling and reduced precipitation in the LGM and warming and enhanced precipitation during the PLIO. The LGM climate shows the largest deviation in annual precipitation from the PI climate, and shows enhanced precipitation in the temperate Andes, and coastal regions for both SE Alaska and the US Pacific Northwest Pacific. Furthermore, LGM precipitation is reduced in the western Himalayas and enhanced in the eastern Himalayas, resulting in a shift of the wettest regional climates eastward along the orogen. The cluster-analysis results also suggest more climatic variability across latitudes east of the Andes in the PLIO climate than in other time-slice experiments conducted here. Taken together, these results highlight significant changes in Late Cenozoic regional climatology over the last ~3 Ma. Finally, we document regions where the largest magnitudes of Late Cenozoic changes in precipitation and temperature occur and offer the highest potential for future observational studies interested in quantifying the impact of climate change on denudation and weathering rates.

Keywords: Cenozoic climate, ECHAM5, Last Glacial Maximum, Mid-Holocene, Pliocene, cluster analysis, Himalaya, Tibet, Andes, Alaska, Cascadia

Earth Surf. Dynam. Discuss., https://doi.org/10.5194/esurf-2017-47
Manuscript under review for journal Earth Surf. Dynam.
Discussion started: 16 August 2017

1. Introduction

Interpretation of orogen denudation histories in the context of climate and tectonic interactions is often hampered by a paucity of terrestrial paleo-climate proxy data needed to reconstruct spatial variations in paleo-climate. Paleo-climate reconstructions are particularly beneficial when denudation rates are determined using geo- and thermo-chronology techniques that integrate over timescales of 10^3-10^{6+} years (e.g. cosmogenic radionuclides or low-temperature thermochronology) [e.g., Kirchner et al., 2001; Schaller et al., 2002; Bookhagen et al., 2005; Moon et al., 2011; Thiede and Ehlers, 2013; Lease and Ehlers, 2013]. However, few studies using denudation rate determination methods that integrate over longer timescales have access to information about past climate conditions that could influence these paleo-denudation rates. Paleo-climate modelling offers an alternative approach to sparsely available proxy data for understanding the spatial and temporal variations in precipitation and temperature in response to changes in orography [e.g. Takahashi and Battisti, 2007a, b; Insel et al., 2010; Feng et al., 2013] and global climate change events [e.g. Salzmann, 2011; Jeffery et al., 2013]. In this study, we characterize the climate at different times in the Cenozoic, and the magnitude of climate change for a range of active orogens. Our emphasis is on identifying changes in climate parameters relevant to weathering and catchment denudation to illustrate the potential importance of various global climate change events on surface processes.

Previous studies of orogen scale climate change provide insight into how different tectonic or global climate change events influence regional climate change. For example, sensitivity experiments demonstrated significant changes in regional and global climate in response to landmass distribution and topography of the Andes, including changes in moisture transport and the north-south asymmetry of the Inter Tropical Convergence Zone [e.g. Takahashi and Battisti, 2007a, Insel et al., 2010]. Another example is the regional and global climate changes induced by the Tibetan Plateau surface uplift due to its role as a cold-temperature island and physical obstacle to circulation [Raymo and Ruddiman, 1992; Kutzbach et al., 1993; Thomas, 1997; Bohner, 2006; Molnar et al., 2010; Boos and Kuang, 2010]. The role of tectonic uplift in long term regional and global climate change remains a focus of research and continues to be assessed with geologic datasets [e.g. Zhisheng, 2001; Dettman et al., 2003] and climate modelling [e.g. Kutzbach et al., 1989; Kutzbach et al., 1993, Bohner, 2006; Takahashi and Battisti, 2007a; Ehlers and Poulsen, 2009; Insel et al., 2010; Boos and Kuang, 2010]. Conversely, climate influences tectonic processes through erosion [e.g. Molnar and England, 1990; Whipple et al., 1999; Montgomery et al., 2001; Willett et al., 2006; Whipple, 2009]. Quaternary climate change between glacial and interglacial conditions [e.g. Braconnot et al., 2007; Harrison et al., 2013] resulted in not only the growth and decay of glaciers and glacial erosion [e.g. Yanites and Ehlers, 2012; Herman et al., 2013; Valla et al., 2011] but also global changes in precipitation and temperature [e.g. Otto-Bliesner et al., 2006; Li et al., 2017] that could influence catchment denudation in non-glaciated environments [e.g. Schaller and Ehlers, 2006; Glotzbach et al., 2013; Marshall et al., 2015]. These dynamics highlight the importance of investigating how much climate has changed over orogens that are focus of studies of climate-tectonic interactions and their impact on erosion.

Despite recognition by previous studies that climate change events relevant to orogen denudation are prevalent throughout the Late Cenozoic, few studies have critically evaluated how different climate change events may, or may not, have affected the orogen climatology, weathering and erosion. Furthermore, recent controversy exists concerning the spatial and temporal scales over which geologic and geochemical observations can record climate-driven changes in weathering and erosion [e.g. Whipple, 2009; von Blanckenburg et al., 2015; Braun, 2016]. This study contributes to our understanding of the interactions between climate, weathering, and erosion by bridging the gap between the paleoclimatology and surface processes communities by documenting the magnitude and distribution of climate change over tectonically active orogens. Our focus is on documenting the magnitude of paleoclimate change in different locations with the intent of informing past and ongoing paleodenudation studies of these regions. The application of

Earth Surf. Dynam. Discuss., https://doi.org/10.5194/esurf-2017-47
Manuscript under review for journal Earth Surf. Dynam.
Discussion started: 16 August 2017

these results to predicted changes in denudation rates is beyond the scope of this study and the focus of future work.

We employ the ECHAM5 global Atmospheric General Circulation Model and document climate change for time slices ranging between the Pliocene (PLIO, ~3 Ma) to pre-industrial (PI) times for the St. Elias Range of South East Alaska, the US Pacific Northwest (Olympic and Cascade Range), western South America (Andes) and South Asia (incl. parts of Central- and East Asia). Our approach is two-fold and includes:

1. An empirical characterization of paleo-climates in these regions based on the covariance and spatial clustering of monthly precipitation and temperature, the monthly change in precipitation and temperature magnitude, and wind speeds where appropriate.

2. Identification of changes in annual mean precipitation and temperature in selected regions over time, specifically from the PLIO to the Last Glacial Maximum (LGM), the Mid-Holocene (MH) and PI.

2. Methods: Climate modeling and cluster analyses for climate characterization

2.1 ECHAM5 simulations

The global Atmospheric General Circulation Model ECHAM5 [Roeckner et al., 2003] has been developed at the Max Planck Institute for Meteorology and is based on the spectral weather forecast model of the ECMWF [Simmons et al., 1989]. In the context of paleoclimate applications, the model has been used mostly at lower resolution (T31, approximately 3.75°x3.75°). The performed studies are not limited to the last millenium [e.g. Jungclaus et al., 2010] but also include research in the field of both warmer and colder climates, at orbital [e.g. Gong et al., 2013; Lohmann et al., 2013; Pfeiffer and Lohmann, 2016; Zhang et al., 2013a; Zhang et al., 2014; Wei and Lohmann, 2012] and tectonic time scales [e.g. Knorr et al., 2011; Stepanek and Lohmann, 2012], and under anthropogenic influence [Gierz et al., 2015].

Here, the ECHAM5 simulations were conducted at a T159 spatial resolution (horizontal grid size ca. 80 km x 80 km at the equator) with 31 vertical levels (between the surface and 10hPa). This high model resolution is admittedly not required for the climatological questions investigated in this study. However, simulations were conducted at this resolution so that future work can apply the results to quantify changes at large catchment to orogen scales. The simulations were conducted for five different time periods: present-day (PD), PI, MH, LGM and PLIO.

A PD simulation (not shown here) was used to establish confidence in the model performance before conducting paleo-simulations and has been compared with the following observation-based datasets: European Centre for Medium-Range Weather Forecasts (ECMWF) re-analyses [ERA40, Uppala et al., 2005], National Centers for Environmental Prediction and National Center for Atmospheric Research (NCEP/NCAR) re-analyses [Kalnay et al., 1996; Kistler et al., 2001], NCEP Regional Reanalysis (NARR) [Mesinger et al., 2006], the Climate Research Unit (CRU) TS3.21 dataset [Harris et al., 2013], High Asia Refined Analysis (HAR30) [Maussion et al., 2014] and the University of Delaware dataset (UDEL v3.01) [Legates et al., 1990]. (See Mutz et al. [2016] for a detailed comparison with a lower resolution model).

The PI climate simulation is an ECHAM5 experiment with PI (reference year 1850) boundary conditions. Sea Surface Temperatures (SST) and Sea Ice Concentration (SIC) are derived from transient coupled ocean-atmosphere simulations [Lorenz and Lohmann, 2004; Dietrich et al., 2013]. Following Dietrich et al. [2013], greenhouse gas (GHG) concentrations are taken from ice core based reconstructions of CO_2 [Etheridge et al., 1996], CH_4 [Etheridge et al., 1998] and N2O [Sowers et al., 2003]. Sea surface boundary conditions for MH originate from a transient, low-resolution, coupled atmosphere-ocean simulation of the mid (6 ka) Holocene [Wei and Lohmann, 2012; Lohmann et al, 2013], where the GHG concentrations are taken from ice core reconstructions of GHG's by Etheridge et al. [1996], Etheridge et al. [1998] and Sowers et al. [2003]. GHG's concentrations for the LGM have been prescribed following

Otto-Bliesner et al. [2006]. Orbital parameters for MH and LGM are set according to Dietrich et al. [2013] and Otto-Bliesner et al. [2006], respectively. LGM land-sea distribution and ice sheet extent and thickness are set based on the PMIP III (Paleoclimate Modelling Intercomparison Project, phase 3) guidelines (elaborated on by Abe-Ouchi et al [2015]). Following Schäfer-Neth and Paul [2003], SST and SIC for the LGM are based on GLAMAP [Sarnthein et al. 2003] and CLIMAP [CLIMAP project members, 1981] reconstructions for the for the Atlantic and Pacific/Indian Ocean, respectively. Global MH and LGM vegetation are based on maps of plant functional types by the BIOME 6000 / Palaeovegetation Mapping Project [Prentice et al., 2000; Harrison et al., 2001; Bigelow et al., 2003; Pickett et al., 2004] and model predictions by Arnold et al. [2009]. Boundary conditions for the PLIO simulation, including GHG concentrations, orbital parameters and surface conditions (SST, SIC, sea land mask, topography and ice cover) are taken from the PRISM (Pliocene Research, Interpretation and Synoptic Mapping) project [Haywood et al., 2010; Sohl et al., 2009; Dowsett et al., 2010]. The PLIO vegetation boundary condition was created by converting the PRISM vegetation reconstruction to the JSBACH plant functional types as described by Stepanek and Lohmann [2012].

The palaeoclimate simulations (PI, MH, LGM, PLIO) using ECHAM5 are carried out for 17 model years, of which the first two years are used for model spin up. The monthly long-term averages (multi-year means for individual months) for precipitation, temperature, as well as precipitation and temperature amplitude, i.e. the mean difference between the hottest and coldest months, have been calculated from the following 15 model years for the analysis presented below.

For further comparison between the simulations, the investigated regions were subdivided (Fig. 1). Western South America was subdivided into four regions: parts of tropical South America (80°-60° W, 23.5-5° S), temperate South America (80°-60° W, 50°-23.5° S), tropical Andes (80°-60° W, 23.5-5° S; high-pass filtered), i.e. most of the Peruvian Andes, Bolivian Andes and northernmost Chilean Andes, and temperate Andes (80°-60° W, 50°-23.5° S, high-pass filtered). South Asia was subdivided into three regions: tropical South Asia (40°-120°E, 0°-23.5°N), temperate South Asia (40°-120°E, 23.5°-60°N), and high altitude South Asia (40°-120°E, 0°-60°N; high-pass filtered).

2.2 Cluster analysis to document temporal and spatial changes in climatology

This section describes the clustering method used in this study. The aim of the clustering approach is to group climate model surface grid boxes together based on similarities in climate. Cluster analyses are statistical tools that allow elements (i) to be grouped by similarities in the elements' attributes. In this study, those elements are spatial units, the elements' attributes are values from different climatic variables, and the measure of similarity is given by a statistical distance. The four basic variables used as climatic attributes of these spatial elements are: near-surface (2m) air temperature, seasonal 2m air temperature amplitude, precipitation rate, and seasonal precipitation rate amplitude. Since monsoonal winds are a dominant feature of the climate in the South Asia region, near surface (10m) speeds of u-wind and v-wind (zonal and meridional wind components, respectively) during the monsoon season (July) and outside the monsoon season (January) are included as additional variables in our analysis of that region. Similarly, u-wind and v-wind speeds during (January) and outside (July) the monsoon season in South America are added to the list of considered variables to take into account the South American Monsoon System (SASM) in the cluster analysis for this region. The long-term monthly means of those variables are used in a hierarchical clustering method, followed by a non-hierarchical k-means correction with randomized re-groupment [Mutz et al., 2016; Wilks, 2011; Paeth, 2004; Bahrenberg et al., 1992].

The hierarchical part of the clustering procedure starts with as many clusters as there are elements (ni), then iteratively combines the most similar clusters to form a new cluster using centroids for the linkage procedure for clusters containing multiple elements. The procedure is continued until the desired number of clusters (k) is reached.

One disadvantage of a pure hierarchical approach is that elements cannot be re-categorized once they are assigned to a cluster, even though the addition of new elements to existing clusters changes the clusters' defining attributes and could warrant a re-categorization of elements. We address this problem by implementation of a (non-hierarchical) k-means clustering correction [e.g. Paeth, 2004]. Elements are re-categorized based on the multivariate centroids determined by the hierarchical cluster analysis in order to minimize the sum of deviations from the cluster centroids. The Mahalanobis distance [e.g. Wilks, 2011] is used as a measure of similarity or distance between the cluster centroids, since it is a statistical distance and thus not sensitive to different variable units. The Mahalanobis distance also accounts for possible multi-collinearity between variables.

The end results of the cluster analyses are subdivisions of the climate in the investigated regions into k subdomains or clusters based on multiple climate variables. The region-specific k has to be prescribed before the analyses. A large k may result in redundant additional clusters describing very similar climates, thereby defeating the purpose of the analysis to identify and describe the dominant, distinctly different climates in the region and their geographical coverage. Since it is not possible to know a priori the ideal number of clusters, k was varied between 3 and 10 for each region and the results presented below identify the optimal number of visibly distinctly different clusters from the analysis.

3. Results

Results from our analysis are first presented for general changes in global temperature and precipitation for the different time slices (Fig. 2, 3), which is then followed by an analysis of changes in the climatology of selected orogens. A more detailed description of temperature and precipitation changes in our selected orogens is presented in subsequent subsections (Fig. 4 and following). All differences in climatology are expressed relative to the PI control run. Changes relative to the PI rather than PD conditions are presented to avoid interpreting an anthropogenic bias in the results and focusing instead on pre-anthropogenic variations in climate. For brevity, near-surface (2m) air temperature and total precipitation rate are referred to as temperature and precipitation.

3.1 Global differences in mean annual temperature

This section describes the differences between simulated MH, LGM, and PLIO annual mean temperature anomalies with respect to PI shown in Fig. 2b, and PI temperature absolute values shown in Fig. 2a. Most temperature differences between the PI and MH climate are within -1°C to 1°C. Exceptions to this are the Hudson Bay, Weddell Sea and Ross Sea regions which experience warming of 1-3°C, 1-5°C and 1-9°C respectively. Continental warming is mostly restricted to low-altitude South America, Finland, western Russia, the Arabian Peninsula (1-3°C) and subtropical north Africa (1-5°C). Simulation results show that LGM and PLIO annual mean temperature deviate from the PI means the most. The global PLIO warming and LGM cooling trends are mostly uniform in direction, but the magnitude varies regionally. The strongest LGM cooling is concentrated in Canada, Greenland, the North Atlantic, Northern Europe and Antarctica. Central Alaska shows no temperature changes, whereas coastal South Alaska experiences cooling of ≤ 9°C. Cooling in the US Pacific northwest is uniform and between 11 and 13°C. Most of high-altitude South America experiences mild cooling of 1-3°C, 3-5°C in the central Andes and ≤ 9°C in the south. Along the Himalayan orogen, LGM temperature values are 5-7°C below PI values. Much of central Asia and the Tibetan plateau cools by 3-5°C, and most of India, low-altitude China and southeast Asia by 1-3°C.

In the PLIO climate, parts of Antarctica, Greenland and the Greenland Sea experience the greatest temperature increase (≤ 19°C). Most of southern Alaska warms by 1-5°C and ≤ 9°C near McCarthy, Alaska. The US Pacific northwest warms by 1-5°C. The strongest warming in South America is concentrated at the Pacific west coast and the

Andes (1-9°C), specifically between Lima and Chiclayo, and along the Chilean-Argentinian Andes south of Bolivia (≤ 9°C). Parts of low-altitude South America to the immediate east of the Andes experience cooling of 1-5°C. The Himalayan orogen warms by 3-9°C, whereas Myanmar, Bangladesh, Nepal, northern India and northeast Pakistan cool by 1-9°C.

3.2 Global differences in mean annual precipitation

Notable differences occur between simulated MH, LGM, PLIO annual mean precipitation anomalies with respect to PI shown in Fig. 3b, and the PI precipitation absolute values shown in Fig. 3a. Of these, MH precipitation deviates the least from PI values. The differences between MH and PI precipitation on land appear to be largest in northern tropical Africa (increase ≤1200 mm/a) and along the Himalayan orogen (increase ≤2000 mm/a) and in central Indian states (decrease) ≤500mm. The biggest differences in western South America are precipitation increases in central Chile between Santiago and Puerto Montt. The LGM climate shows the largest deviation in annual precipitation from the PI climate, and precipitation on land mostly decreases. Exceptions are increases in precipitation rates in North American coastal regions, especially in coastal South Alaska (≤2300 mm/a) and the US Pacific Northwest (≤1700 mm/a). Further exceptions are precipitation increases in low-altitude regions immediately east of the Peruvian Andes (≤1800 mm/a), central Bolivia (≤1000 mm/a), most of Chile (≤1000 mm/a) and northeast India (≤1900 mm/a). Regions of notable precipitation decrease are northern Brazil (≤1700 mm/a), southernmost Chile and Argentina (≤1900 mm/a), coastal south Peru (≤700 mm/a), central India (≤2300 mm/a) and Nepal (≤1600 mm/a).

Most of the precipitation on land in the PLIO climate is higher than those in the PI climate. Precipitation is enhanced by ca. 100-200 mm/a in most of the Atacama desert, by ≤1700 mm/a south of the Himalayan orogen and by ≤1400 mm/a in tropical South America. Precipitation significantly decreases in central Peru (≤2600mm), southernmost Chile (≤2600mm) and from eastern Nepal to northernmost northeast India (≤2500mm).

3.3 Paleoclimate characterization from the cluster analysis and changes in regional climatology

In addition to the above described global changes, the PLIO to PI regional climatology changes substantially in the four investigated regions of: South Asia (section 3.3.1), the Andes (section 3.3.2), South Alaska (section 3.3.3) and the Cascade Range (section 3.3.4). Each climate cluster defines separate distinct climate that is characterized by the mean values of the different climate variables used in the analysis. The clusters are calculated by taking the arithmetic means of all the values (climatic means) calculated for the grid boxes within each region. The regional climates are referred to by their cluster number C_1, C_2, …, C_k, where *k* is the number of clusters specified for the region. The clusters for specific paleo-climates are mentioned in the text as $C_{i(t)}$, where *i* corresponds to the cluster number (*i*=1, …, *k*) and *t* to the simulation time period (*t*=PI, MH, LGM, PLIO). The descriptions first highlight the similarities and then the differences in regional climate. The cluster means of seasonal near-surface temperature amplitude and seasonal precipitation amplitude are referred to as temperature and precipitation amplitude. The median, 25th percentile, 75th percentile, minimum and maximum values for annual mean precipitation are referred to as P_{md}, P_{25}, P_{75}, P_{min} and P_{max} respectively. Likewise, the same statistics for temperature are referred to as $T_{md,}$ T_{25}, T_{75}, T_{min} and T_{max}. These are presented as boxplots of climate variables in different time periods. When the character of a climate cluster is described as “high”, “moderate” and “low”, the climatic attribute’s values are described relative to the value range of the specific region in time, thus high PLIO precipitation rates may be higher than high LGM precipitation rates. The character is presented a raster plots, to allow compact visual representation of it. The actual mean values for each variable in every time-slice and region-specific cluster are included in tables in the supplementary material.

3.3.1 Climate change and paleoclimate characterization in South Asia, Central- and East Asia

This section describes the regional climatology of the four investigated Cenozoic time slices and how precipitation and temperature changes from PLIO to PI times in tropical, temperate and high altitude regions. LGM and PLIO simulations show the largest simulated temperature and precipitation deviations (Fig. 4b) from PI temperature and precipitation (Fig. 4a) in the South Asia region. LGM temperatures are 1-7°C below PI temperatures and the direction of deviation is uniform across the study region. PLIO temperature is mostly above PI temperatures by 1-7°C. The cooling of 3-5°C in the region immediately south of the Himalayan orogen represents one of the few exceptions. Deviations of MH precipitation from PI precipitation in the region are greatest along the eastern Himalayan orogeny, which experiences an increase in precipitation (≤2000 mm/a). The same region experiences a notable decrease in precipitation in the LGM simulation, which is consistent in direction with the prevailing precipitation trend on land during the LGM. PLIO precipitation on land is typically higher than PI precipitation.

Annual means of precipitation and temperature spatially averaged for the regional subdivisions and the different time slice simulations have been compared. The value range P_{25} to P_{75} of precipitation is higher for tropical South Asia than for temperate and high altitude South Asia (Fig. 5 a-c). The LGM values for P_{25}, P_{md} and P_{75} are lower than for the other time slice simulations, most visibly for tropical South Asia (ca. 100 mm/a). The temperature range (both T_{75}-T_{25} and T_{max}- T_{min}) is smallest in the hot (ca. 21°C) tropical South Asia, wider in the high altitude (ca. -8°C) South Asia, and widest in the temperate (ca. 2°C) South Asia region (Fig. 5 d-f). T_{md}, T_{25} and T_{75} values for the LGM are ca. 1°C, 1-2°C and 2°C below PI and MH temperatures in tropical, temperate and high altitude South Asia respectively, whereas the same temperature statistics for the PLIO simulation are ca. 1°C above PI and MH values in all regional subdivisions (Fig. 5 d-f). With respect to PI and MH values, precipitation and temperature are generally lower in the LGM and higher in the PLIO in tropical, temperate and high altitude South Asia.

In all time periods, the wettest climate cluster C_1 covers an area along the southeastern Himalayan orogen (Fig. 6 a-d) and is defined by the highest precipitation amplitude (dark blue, Fig. 6 e-h). $C_{5(PI)}$, $C_{3(MH)}$, $C_{4(LGM)}$ and $C_{5(PLIO)}$ are characterized by (dark blue, Fig. 6e-h) the highest temperatures, u-wind and v-wind speeds during the summer monsoon in their respective time periods, whereas $C_{4(PI)}$, $C_{5(MH)}$, and $C_{6(LGM)}$ are defined by low temperatures and highest temperature amplitude, u-wind and v-wind speeds outside the monsoon season (in January) in their respective time periods (Fig. 6 e-h). The latter 3 climate classes cover much of the more continental, northern landmass in their respective time periods and represents a cooler climate affected more by seasonal temperature fluctuations (Fig. 6 a-d). The two wettest climate clusters C_1 and C_2 are more restricted to the eastern end of the Himalayan orogen in the LGM than during other times, indicating that the LGM precipitation distribution over the South Asia landmass is more concentrated in this region than in other time slice experiments.

3.3.2 Climate change and paleoclimate characterization in the Andes, Western South America

This section describes the cluster analysis based regional climatology of the four investigated Late Cenozoic time slices and illustrates how precipitation and temperature changes from PLIO to PI in tropical and temperate low- and high altitude (i.e. Andes) regions in western South America (Fig. 7-9).

LGM and PLIO simulations show the largest simulated deviations (Fig. 7b) from PI temperature and precipitation (Fig. 7a) in western South America. The direction of LGM temperature deviations from PI temperatures is negative and uniform across the region. LGM temperatures are typically 1-3°C below PI temperatures across the region, and 1-7°C below PI values in the Peruvian Andes, which also experience the strongest and most widespread increase in precipitation during the LGM (≤1800 mm/a). Other regions, such as much of the northern Andes and tropical South America, experience a decrease of precipitation in the same experiment. PLIO temperature is mostly elevated above PI temperatures by 1-5°C. The Peruvian Andes experience a decrease in precipitation (≤2600mm), while the northern Andes are wetter in the PLIO simulation compared to the PI control simulation.

PI, MH, LGM and PLIO precipitation and temperature means for regional subdivisions have been compared. The P_{25} to P_{75} range is smallest for the relatively dry temperate Andes and largest for tropical South America and the tropical Andes (Fig. 8 a-d). P_{max} is lowest in the PLIO in all four regional subdivisions even though P_{md}, P_{25} and P_{75} in the PLIO simulation are similar to the same statistics calculated for PI and MH time slices. P_{md}, P_{25} and P_{75} for the LGM are ca. 50 mm/a lower in tropical South America and ca. 50 mm/a higher in the temperate Andes. Average PLIO temperatures are slightly warmer and LGM temperatures are slightly colder than PI and MH temperatures in tropical and temperate South America (Fig. 8 e and f). These differences are more pronounced in the Andes, however. T_{md}, T_{25} and T_{75} are ca. 5°C higher in the PLIO climate than in PI and MH climates in both temperate and tropical Andes, whereas the same temperatures for the LGM are ca. 2-4°C below PI and MH values (Fig. 8 g and h).

For the LGM, the model computes drier-than-PI conditions in tropical South America and tropical Andes, enhanced precipitation in the temperate Andes, and a decrease in temperature that is most pronounced in the Andes. For the PLIO, the model predicts precipitation similar to PI, but with lower precipitation maxima. PLIO temperatures generally increase from PI temperatures, and this increase is most pronounced in the Andes.

The climate variability in the region is described by six different clusters (Fig. 9 a-d), which have similar attributes in all time periods. The wettest climate C_1 is also defined by moderate to high precipitation amplitudes, low temperatures and moderate to high u-wind speeds in summer and winter in all time periods (dark blue, Fig. 9 e-h). $C_{2(PI)}$, $C_{2(MH)}$, $C_{3(LGM)}$ and $C_{2(PLIO)}$ are characterized by high temperatures and low seasonal temperature amplitude (dark blue, Fig. 9 e-h), geographically cover the north of the investigated region, and represent a more tropical climate. $C5_{(PI)}$, $C5_{(MH)}$, $C6_{(LGM)}$ and $C6_{(PLIO)}$ are defined by low precipitation and precipitation amplitude, high temperature amplitude and high u-wind speeds in winter (Fig. 9 e-h), cover the low-altitude south of the investigated region (Fig. 9 a-d) and represent dry, extra-tropical climates with more pronounced seasonality. In the PLIO simulation, the lower-altitude east of the region has four distinct climates, whereas the analysis for the other time slice experiments only yield three distinct climates for the same region.

3.3.3 Climate change and paleoclimate characterization in the St. Elias Range, Southeast Alaska

This section describes the changes in climate and the results from the cluster analysis for South Alaska (Fig. 10-12). As is the case for the other study areas, LGM and PLIO simulations show the largest simulated deviations (Fig. 10b) from PI temperature and precipitation (Fig. 10a). The sign of LGM temperature deviations from PI temperatures is negative and uniform across the region. LGM temperatures are typically 1-9°C below PI temperatures, with the east of the study area experiencing largest cooling. PLIO temperatures are typically 1-5°C above PI temperatures and the warming is uniform for the region. In comparison to the PI simulation, LGM precipitation is lower on land, but higher (≤2300mm) in much of the coastal regions of South Alaska. Annual PLIO precipitation is mostly higher (≤800mm) than for PI.

P_{md}, P_{25}, P_{75}, P_{min} and P_{max} for South Alaskan mean annual precipitation do not differ much between PI, MH and PLIO climates, while P_{md}, P_{25}, P_{75} and P_{min} decrease by ca. 20-40 mm/a and P_{max} increases during the LGM (Fig. 11a). The Alaskan PLIO climate is distinguished from the PI and MH climates by its higher (ca. 2°C) regional temperature means, T_{25}, T_{75} and T_{md} (Fig. 11b). Mean annual temperatures, T_{25}, T_{75}, T_{min} and T_{max} are lower in the LGM than in any other considered time period (Fig. 11b), and about 3-5°C lower than during the PI and MH.

Distinct climates are present in the PLIO to PI simulations for Southeast Alaska. Climate cluster C_1 is always geographically restricted to coastal southeast Alaska (Fig. 12 a-d) and characterized by the highest precipitation, precipitation amplitude, temperature, and by relatively low temperature amplitude (dark blue, Fig. 12 e-h). Climate C_2 is characterized by moderate to low precipitation, precipitation amplitude, temperature, and by low temperature amplitude. C_2 is either restricted to coastal southeast Alaska (in MH and LGM climates) or coastal southern Alaska (in PI and PLIO climates). Climate C_3 is described by low precipitation, precipitation amplitude, temperature, and moderate temperature amplitude in all simulations. It covers coastal western Alaska and separates climate C_1 and C_2 from the northern C_4 climate. Climate C_4 is distinguished by the highest mean temperature amplitude, by low temperature and precipitation amplitude, and by lowest precipitation.

The geographical ranges of PI climates C_1- C_4 and PLIO climates C_1- C_4 are similar. $C_{1(PI/PLIO)}$ and $C_{2(PI/PLIO)}$ spread over a larger area than $C_{1(MH/LGM)}$ and $C_{2(MH/LGM)}$. $C_{2(PI/PLIO)}$ are not restricted to coastal southeast Alaska, but also cover the coastal southwest of Alaska. The main difference in characterization between PI and PLIO climates C_1- C_4 lies in the greater difference (towards lower values) in precipitation, precipitation amplitude and temperature from $C_{1(PLIO)}$ to $C_{2(PLIO)}$ compared to the relatively moderate decrease in those means from $C_{1(PI)}$ to $C_{2(PI)}$.

3.3.4 Climate change and paleoclimate characterization in the Cascade Range, US Pacific Northwest

This section describes the character of regional climatology in the US Pacific Northwest and its change over time (Fig. 13-15). The region experiences cooling of typically 9-11°C on land during the LGM, and warming of 1-5°C during the PLIO (Fig. 13b) when compared to PI temperatures (Fig. 13a). LGM precipitation increases over water, decreases on land by ≤800 mm/a in the North and in the vicinity of Seattle and increases on land by ≤1400 mm/a on Vancouver Island, around Portland and the Olympic Mountains, whereas PLIO precipitation does not deviate much from PI values over water and varies in the direction of deviation on land. MH temperature and precipitation deviation from PI values are negligible.

P_{md}, P_{25}, P_{75}, P_{min} and P_{max} for the Cascade Range do not notably differ between the four time periods (Fig. 14a). The LGM range of precipitation values is slightly larger than that of the PI and MH with slightly increased P_{md}, while the respective range is smaller for simulation PLIO. The T_{md}, T_{25}, T_{75} and T_{max} values for the PLIO climate are ca. 2°C higher than those values for PI and MH (Fig. 14b). All temperature statistics for the LGM are notably (ca. 13°C) below their analogues in the other time periods (Fig. 14b).

PI, LGM and PLIO clusters are similar in both their geographical patterns (Fig. 15 a, c, d) and their characterization by mean values (Fig. 15 e, g, h). C_1 is the wettest cluster and shows the highest amplitude in precipitation. The common characteristics of the C_2 cluster are moderate to high precipitation and precipitation amplitude. C_4 is characterized by the lowest precipitation and precipitation amplitudes, and the highest temperature amplitudes. Regions assigned to clusters C_1 and C_2 are in proximity to the coast, whereas C_4 is geographically restricted to more continental settings.

In the PI and LGM climates, the wettest cluster C_1 is also characterized by high temperatures (Fig 10 e, g). However, virtually no grid boxes were assigned to $C_{1(LGM)}$. $C_{1(MH)}$ differs from other climate state's C_1 clusters in that it is also described by moderate to high near surface temperature and temperature amplitude (Fig 10 f), and in that it is geographically less restricted and, covering much of Vancouver Island and the continental coastline north of it (Fig 10 b). Near surface temperatures are highest for C_2 in PI, LGM and PLIO climates (Fig 10 e, g, h) and low for $C_{2(MH)}$ (Fig 10 f). $C_{2(MH)}$ is also geographically more restricted than C_2 clusters in PI, LGM and PLIO climates (Fig 10 a-d). $C_{2(PI)}$, $C_{2(MH)}$ and $C_{2(LGM)}$ have a low temperature amplitude (Fig 10 e-g), whereas $C_{2(PLIO)}$ is characterized by a moderate temperature amplitude (Fig 10 h).

4. Discussion

In the following, we synthesize our results and compare to previous studies that investigate the effects of temperature and precipitation change on erosion. When possible, we relate the magnitude of climate change predicted in each geographical study area with terrestrial proxy data.

4.1 Synthesis of temperature changes and implications for weathering and erosion

Changes in temperature can affect physical weathering due to temperature-induced changes in periglacial processes and promote frost cracking and frost creep [e.g., Matsuoka, 2001; Schaller et al., 2002; Matsuoka and Murton, 2008; Delunel et al., 2010; Marshall et al., 2015], and also biotic weathering and erosion [e.g. Moulton et al., 1998; Banfield et al., 1999; Dietrich and Perron, 2006]. Quantifying and understanding past changes in temperature is thus vital for our understanding of denudation histories. In the following, we highlight regions in the world where future observational studies might be able to document significant warming or cooling that would influence temperature related changes in physical and chemical weathering over the last ~3 Ma.

Simulated MH temperatures show little deviation (typically < 1°C) from PI temperatures in the investigated regions (Fig. 2b), suggesting little difference in MH temperature-related weathering. LGM cooling is accentuated at the poles, in general agreement with studies such as Otto-Bliesner et al. [2006] and Braconnot et al. [2007], and increases the equator-to-pole pressure gradient and consequently strengthens global atmospheric circulation. Despite this global trend, cooling in coastal South Alaska is higher (≤ 9°C) than in central Alaska (0±1°C). Cooling in most of the lower-latitude regions in South America and central to southeast Asia is relatively mild. The Tibetan plateau experiences more cooling (3-5°C) than adjacent low-altitude regions (1-3°C) during the LGM.

The PLIO simulation shows little to no warming in the tropics and accentuated warming at the poles, as do findings of Salzmann et al. [2011] and Robinson [2009] and Ballantyne [2010] respectively. This would reduce the equator-to-pole sea and land surface temperature gradient, as also reported by Dowsett et al. [2010], and also weaken global atmospheric circulation. Agreement with proxy-based reconstructions, as is the case of the relatively little warming in lower latitudes, is not surprising given that sea surface temperature reconstructions are prescribed in this uncoupled atmosphere simulation. It should be noted that coupled ocean-atmosphere simulations do predict more low-latitude warming [e.g. Stepanek and Lohmann 2012; Zhang et al. 2013b].

Warming in simulation PLIO is present in parts of Canada and Greenland (up to 19°C) and consistent with values based on multi-proxy studies [Ballantyne et al., 2010]. Due to a scarcity of paleo-botanical proxies in Antarctica, reconstruction-based temperature and ice-sheet extent estimates for a PLIO climate have high uncertainties [Salzmann et al., 2011], making model validation difficult. Furthermore, controversy about relatively little warming in the south polar regions compared to the north polar regions remains [e.g. Hillenbrand and Fütterer, 2002; Wilson et al., 2002]. Mid-latitude PLIO warming is mostly in the 1-3°C range with notable exceptions of cooling in the northern tropics of Africa and on the Indian subcontinent, especially south of the Himalayan orogen. The warming in simulation PLIO in South Alaska and the US Pacific northwest is mostly uniform and in the range of 1-5°C, whereas warming in South America is concentrated at the Pacific west coast and the Andes between Lima and Chiclayo, and along the Chilean-Argentinian Andes south of Bolivia (≤ 9°C).

Overall, annual mean temperatures in the MH simulation show little deviation from PI values. The more significant temperature deviations of the colder LGM and of the warmer PLIO simulations are accentuated at the poles leading to higher and lower equator-to-pole temperature gradients respectively. The largest temperature-related changes (relative to PI conditions) in weathering and subsequent erosion are therefore to be expected in the LGM and PLIO climates.

4.2 Synthesis of precipitation changes and implications for orogen denudation

Changes in precipitation affects erosion through river incision, sediment transport, and erosion due to extreme precipitation events and storms [e.g. Whipple and Tucker, 1999; Hobley et al., 2010]. Furthermore, vegetation type and cover also co-evolve with variations in precipitation and with changes in geomorphology [e.g. Marston 2010; Roering et al., 2010]. These vegetation changes in turn modify hillslope erosion by increasing root mass and canopy cover, and decreasing water-induced erosion via surface runoff [e.g. Gyssels et al., 2005]. Therefore, understanding and quantifying changes in precipitation in different paleo-climates is necessary for a more complete reconstruction of orogen denudation histories. A synthesis of predicted precipitation changes is provided below, and highlights regions where changes in river discharge and hillslope processes might be impacted by climate change over the last ~3 Ma.

Simulated MH precipitation rates show little deviation from the PI in most of the investigated regions, suggesting little difference in MH precipitation-related erosion. The Himalayan orogen is an exception and shows a precipitation increase of ≤2000 mm/a. The climate's enhanced erosion potential, that could result from such a climatic change, should be taken into consideration when paleo-erosion rates estimated from the geological record in this area are interpreted [e.g. Bookhagen et al., 2005]. Specifically, higher precipitation rates (along with differences in other rainfall-event parameters) could increase the probability of mass movement events on hillslopes, especially where hillslopes are close to the angle of failure [e.g. Montgomery, 2001], and modify fluxes to increase shear stresses exerted on river beds and increase stream capacity to enhance erosion on river beds (e.g. by abrasion).

Most precipitation on land is decreased during the LGM due to large-scale cooling and decreased evaporation over the tropics, resulting in an overall decrease in inland moisture transport [e.g., Braconnot et al. 2007]. Coastal North America, the investigated US Pacific Northwest and the southeastern coast of Alaska are exceptions in that there is strongly enhanced precipitation of ≤1700 mm/a and ≤2300 mm/a, respectively. Reduced precipitation in other parts of southern Alaska result in a stronger south-to-north drying gradient than in the PI simulation. This could result in more regionally differentiated variations in precipitation-specific erosional processes in the St. Elias Range rather than causing systematic offsets for the LGM. Although precipitation is significantly reduced along much of the Himalayan orogen (≤1600 mm/a), which is consistent with findings by, e.g., Braconnot et al. [2007], northeast India experiences strongly enhanced precipitation (≤1900 mm/a). This could have large implications for studies of uplift and erosion at orogen syntaxes, where highly localized and extreme denudation has been documented [e.g. Koons et al., 2013; Bendick and Ehlers, 2014].

Overall, the PLIO climate is wetter than the PI climate, in particular in the (northern) mid-latitudes, and possibly related to a northward shift of the northern Hadley cell boundary that is ultimately the result of a reduced equator-to-pole temperature gradient [e.g. Haywood et al. 2000, 2013; Dowsett et al. 2010]. A reduction of this gradient by ca. 5°C is indeed present in the PLIO simulation of this study (Fig. 2b). Most of the PLIO precipitation over land increases during the PLIO. This finding agrees well with simulations performed at a lower spatial model resolution [cf. Stepanek and Lohmann, 2012]. PLIO precipitation significantly increases at the Himalayan orogen by ≤1400 mm/a and decreases from eastern Nepal to Namcha Barwa (≤2500 mm/a). Most of the Atacama Desert experiences an increase in precipitation by 100-200 mm/a, which may have to be considered in erosion and uplift history reconstructions for the Andes. A significant increase (~2000 mm/a) in precipitation from simulation PLIO to modern conditions is simulated for the eastern margin of the Andean Plateau in Peru and for northern Bolivia. This is consistent with recent findings of a pulse of canyon incision in these locations in the last ~3 Ma [Lease and Ehlers, 2013].

Overall, the simulated MH precipitation varies least from PI precipitation. The LGM is generally drier than the PI simulation, even though pockets of a wetter-than-PI climate do exist, such as much of coastal North America. Extra-tropical increased precipitation of the PLIO simulation and decreased precipitation of the LGM climate may be the result of decreased and increased equator-to-pole temperature gradients, respectively.

4.3 Trends in Late Cenozoic changes in regional climatology

This section describes the major changes in regional climatology and highlights their possible implications on erosion rates.

Himalaya-Tibet, South Asia

In South Asia, cluster-analysis based categorization and description of climates (Fig. 6) remains similar throughout time. However, the two wettest climates (C_1 and C2) are geographically more restricted to the eastern Himalayan orogen in the LGM simulation. Even though precipitation over the South Asia region is generally lower, this shift indicates that rainfall on land is more concentrated in this region and that the westward drying gradient along the orogen is more accentuated than during other time periods investigated here. While there is limited confidence in the global Atmospheric General Circulation Model's abilities to accurately represent meso-scale precipitation patterns [e.g. Cohen 1990], the simulation warrants careful consideration of possible, geographically non-uniform offsets in precipitation in investigations of denudation and uplift histories.

MH precipitation and temperature in tropical, temperate and high-altitude South Asia is similar to PI precipitation and temperature, whereas LGM precipitation and temperatures are generally lower (by ca. 100 mm/a and 1-2°C respectively), possibly reducing precipitation-driven erosion and enhancing frost-driven erosion in areas pushed into a near-zero temperature range during the LGM.

Andes, South America

Clusters in South America (Fig. 9), which are somewhat reminiscent of the Köppen and Geiger classification [Kraus, 2001], remain mostly the same over the last 3 Ma. In the PLIO simulation, the lower-altitude east of the region is characterized by four distinct climates, which suggests enhanced latitudinal variability in the PLIO climate compared to PI with respect temperature and precipitation.

The largest temperature deviations from PI values are derived for the PLIO simulation in the (tropical and temperate) Andes, where temperatures exceed PI values by 5°C. On the other hand, LGM temperatures in the Andes are ca. 2-4°C below PI values in the same region (Fig 7 g and h). In the LGM simulation, tropical South America experiences ca. 50 mm/a less precipitation, the temperate Andes receive ca. 50 mm/a more precipitation than in PI and MH simulations. These latitude-specific differences in precipitation changes ought to be considered in attempts to reconstruct precipitation-specific paleo-erosion rates in the Andes on top of longitudinal climate gradients highlighted by, e.g., Montgomery et al. [2001].

St. Elias Range, South Alaska

South Alaska is subdivided into two wetter and warmer clusters in the south, and two drier, colder clusters in the north. The latter are characterized by increased seasonal temperature variability due to being located at higher latitudes (Fig. 12). The different equator-to-pole temperature gradients for LGM and PLIO may affect the intensity of the Pacific North American Teleconnection (PNA), which has significant influence on temperatures and precipitation, especially in southeast Alaska, and may in turn result in changes in regional precipitation and temperature patterns. While this appears to be a robust feature for the considered climate states, and hence over the recent geologic history, the LGM sets itself apart from PI and MH climates by generally lower precipitation (20-40 mm) and lower temperatures (3-5°C, Fig. 10, 11), which may favour frost driven weathering during glacial climate states [e.g. Marshall et al. 2015]. Simulation PLIO is distinguished by temperatures that exceed PI and MH conditions by ca. 2°C, and by larger temperature and precipitation value ranges, possibly modifying temperature- and precipitation-dependent erosional processes in the region of South Alaska.

Cascade Range, US Pacific Northwest

In all time slices, the geographic climate patterns, based on the cluster analysis (Fig. 15), represents an increase in the degree of continentality from the wetter coastal climates to the further inland located climates with greater seasonal temperature amplitude and lower precipitation and precipitation amplitude (Fig 15 e-h). The most notable difference between the time slices is the strong cooling during the LGM, when temperatures are ca. 13°C (Fig. 13, 14) below those of other time periods, possibly leading to enhanced sediment production driven by frost processes, as proposed for parts of the Pacific Northwest by Marshall et al. [2015].

4.4 Conclusions

We present a cluster-analysis-based description of the geographic coverage of possible distinct regional expressions of climates from four different time slices (Fig. 6, 9, 12, 15). These are determined with respect to a selection of variables that characterize the climate of the region and may be relevant to weathering and erosional processes. While the geographical climate patterns remain similar throughout time (as indicated by results of four different climate states representative for the climate of the last 3 Ma), results for the PLIO simulation suggests more climatic variability east of the Andes (with respect to near-surface temperature, seasonal temperature amplitude, precipitation, seasonal precipitation amplitude and seasonal u-wind and v-wind speeds). Furthermore, the wetter climates in the South Asia region retreat eastward along the Himalayan orogen for the LGM simulation, this is due to decreased precipitation along the western part of the orogen and enhanced precipitation on the eastern end, possibly signifying more localised high erosion rates.

Most global trends of the high-resolution LGM and PLIO simulations conducted here are in general agreement with previous studies [Otto-Bliesner et al., 2006; Braconnot et al., 2007; Wei and Lohmann, 2012; Lohmann et al., 2013; Zhang et al., 2013b, 2014; Stepanek and Lohmann, 2012]. The MH does not deviate notably from the PI, the LGM is relatively dry and cool, while the PLIO is comparably wet and warm. While the simulated regional changes in temperature and precipitation usually agree with the sign of the simulated global changes, there are region-specific differences in the magnitude and direction. For example, the LGM precipitation of the Tropical Andes does not deviate significantly from PI precipitation, whereas LGM precipitation in the Temperate Andes is enhanced.

The changes in regional climatology presented here are manifested, in part, by small to large magnitude changes in fluvial and hillslope relevant parameters such as precipitation and temperature. For the regions investigated here we find that precipitation differences between the PI, MH, LGM, and PLIO are in many areas around +/- 200-600 mm/yr, and locally can reach maximums of +/- 1000-2000 mm/yr (Figs. 4, 7, 10, 13). Temperature differences between these same time periods are around 1-4 °C in many places, but reach maximum values of 8-10 °C. The magnitude of these differences are not trival, and will likely impact fluvial and hillslope erosion and sediment transport, as well as biotic and abiotic weathering. The regions of large magnitude changes in precipitation and temperature documented here (Figs. 4, 7, 10, 13) offer the highest potential for future observational studies interested in quantifying the impact of climate change on denudation and weathering rates.

Acknowledgements

This study was supported by European Research Council (ERC) Consolidator Grant number 615703 to T. Ehlers. We thank B. Adams and J. Starke for constructive discussions. The DKRZ is thanked for computer time used for some of the simulations presented here. C. Stepanek, M. Werner, and G. Lohmann acknowledge funding by the Helmholtz Climate Initiative Reklim and the Alfred Wegener Institute's research programme Marine, Coastal and Polar Systems.

Figure Captions

Figure 1 Topography for regions (a) tropical South Asia, (b) temperate South Asia, (c) high altitude South Asia, (d) temperate South America, (e) tropical South America, (f) temperate Andes, (g) tropical Andes.

Figure 2 Global PI annual mean near-surface temperatures (a), and deviations of MH, LGM and PLIO annual mean near-surface temperatures from PI values (b). Units are °C and insignificant ($p < 99\%$) differences (as determined by a t-test) are greyed out.

Figure 3 Global PI annual mean precipitation (a), and deviations of MH, LGM and PLIO annual mean near-surface temperatures from PI values (b). Units are mm/yr.

Figure 4 PI annual mean near-surface temperatures (a), and deviations of MH, LGM and PLIO annual mean near-surface temperatures from PI values (b) for the South Asia region. Insignificant ($p < 99\%$) differences (as determined by a t-test) are greyed out.

Figure 5 PI, MH, LGM and PLIO annual mean precipitation in (a) tropical South Asia, (b) temperate South Asia, and (c) high-altitude South Asia; PI, MH, LGM and PLIO annual mean temperatures in (d) tropical South Asia, (e) temperate South Asia, and (f) high-altitude South Asia. For each time slice, the minimum, lower 25th percentile, median, upper 75th percentile and maximum are plotted.

Figure 6 Geographical coverage and characterization of climate classes C_1- C_6 based on cluster-analysis of 8 variables (near surface temperature, seasonal near surface temperature amplitude, total precipitation, seasonal precipitation amplitude, u-wind in January and July, v-wind in January and July) in the South Asia region. The geographical coverage of the climates C_1- C_6 is shown on the left for PI (a), MH (b), LGM (c) and PLIO (d); the complementary, time-slice specific characterization of C_1- C_6 for PI (e), MH (f), LGM (g) and PLIO (h) is shown on the right.

Figure 7 PI annual mean near-surface temperatures (a), and deviations of MH, LGM and PLIO annual mean near-surface temperatures from PI values (b) for western South America. Insignificant ($p < 99\%$) differences (as determined by a t-test) are greyed out.

Figure 8 PI, MH, LGM and PLIO annual mean precipitation in (a) tropical South America, (b) temperate South America, (c) tropical Andes, and (d) temperate Andes; PI, MH, LGM and PLIO annual mean temperatures in (e) tropical South America, (f) temperate South America, (g) tropical Andes, and (h) temperate Andes. For each time slice, the minimum, lower 25th percentile, median, upper 75th percentile and maximum are plotted.

Earth Surf. Dynam. Discuss., https://doi.org/10.5194/esurf-2017-47
Manuscript under review for journal Earth Surf. Dynam.
Discussion started: 16 August 2017

Figure 9 Geographical coverage and characterization of climate classes C_1- C_6 based on cluster-analysis of 8 variables (near surface temperature, seasonal near surface temperature amplitude, precipitation, seasonal precipitation amplitude, u-wind in January and July, v-wind in January and July) in western South America. The geographical coverage of the climates C_1- C_6 is shown on the left for PI (a), MH (b), LGM (c) and PLIO (d); the complementary, time-slice specific characterization of C_1- C_6 for PI (e), MH (f), LGM (g) and PLIO (h) is shown on the right.

Figure 10 PI annual mean near-surface temperatures (a), and deviations of MH, LGM and PLIO annual mean near-surface temperatures from PI values (b) for the South Alaska region. Insignificant ($p < 99\%$) differences (as determined by a t-test) are greyed out.

Figure 11 PI, MH, LGM and PLIO annual mean precipitation (a), and mean annual temperatures (b) in South Alaska. For each time slice, the minimum, lower 25th percentile, median, upper 75th percentile and maximum are plotted.

Figure 12 Geographical coverage of climate classes C_1- C_4 based on cluster-analysis of 4 variables (near surface temperature, seasonal near surface temperature amplitude, total precipitation, seasonal total precipitation amplitude) in southern Alaska. The geographical coverage of the climates C_1- C_4 is shown on the left for PI (a,), MH (b), LGM (c) and PLIO (d); the complementary, time-slice specific characterization of C_1- C_6 for PI (e), MH (f), LGM (g) and PLIO (h) is shown on the right.

Figure 13 PI annual mean near-surface temperatures (a), and deviations of MH, LGM and PLIO annual mean near-surface temperatures from PI values (b) for the US Pacific Northwest. Insignificant ($p < 99\%$) differences (as determined by a t-test) are greyed out.

Figure 14 PI, MH, LGM and PLIO annual mean precipitation (a), and annual mean temperatures (b) in the Cascades, US Pacific Northwest. For each time slice, the minimum, lower 25th percentile, median, upper 75th percentile and maximum are plotted.

Figure 15 Geographical coverage and characterization of climate classes C_1- C_4 based on cluster-analysis of 4 variables (near surface temperature, seasonal near surface temperature amplitude, total precipitation, seasonal total precipitation amplitude) in the Cascades, US Pacific Northwest. The geographical coverage of the climates C_1- C_4 is shown on the left for PI (a), MH (b), LGM (c) and PLIO (d); the complementary, time-slice specific characterization of C_1- C_6 for PI (e), MH (f), LGM (g) and PLIO (h) is shown on the right.

Earth Surf. Dynam. Discuss., https://doi.org/10.5194/esurf-2017-47
Manuscript under review for journal Earth Surf. Dynam.
Discussion started: 16 August 2017

References

Abe-Ouchi, A., Saito, F., Kageyama, M., Bracannot, P., Harrison, S. P., Lambeck, K., Otto-Bliesner, B. L., Peltier, W.R., Tarasov, L., Peterschmitt, J.-Y., Takahashi, K.: Ice-sheet configuration in the CMUP5/PMIP3 Last Glacial Maximum experiments. *Geosci. Model Dev.*, 8, 3621-3637, doi:10.5194/gmd-8-3621-2015, 2015

Arnold, L., Breon, F.M., and Brewer, S: The earth as an extrasolar planet: the vegetation spectral signature today and during the last Quaternary climatic extrema, *Int. J. Astrobiol.*, 8, 81–94. http://dx.doi.org/10.1017/S1473550409004406, 2009.

Bahrenberg , G., Giese, E., and Nipper, J.: Multivariate Statistik. *Statistische Methoden in der Geographie 2*, Stuttgart, 1992.

Ballantyne, A.P., Greenwood, D.R., Sinninghe Damste, J.S., Csank, A.Z., Eberle, J.J., and Rybczynski, N.: Significantly warmer Arctic surface temperatures during the Pliocene indicated by multiple independent proxies, *Geology* 38 (7), 603–606, 2010.

Banfield, J.F., Barker, W.W., Welch, S.A., and Taunton, A.: Biological impact on mineral dissolution: application of the lichen model to understanding mineral weathering in the rhizophere, *Proceedings of the National Academy of Sciences*, 96, 3404-3411, 1999.

Bendick, R., and Ehlers, T.A.: Extreme localized exhumation at syntaxes initiated by subduction geometry, *Geophys. Res. Lett.*, *41*(16), 2014GL061026, doi:10.1002/2014GL061026, 2014.

Bigelow, N. H., Brubaker, L. B., Edwards, M. E., Harrison, S. P., Prentice, I. C., Anderson, P. M., Andreev, A. A., Bartlein, P. J., Christensen, T. R., Cramer, W., Kaplan, J. O., Lozhkin, A. V., Matveyeva, N. V., Murray, D. V., McGuire, A. D., Razzhivin, V. Y., Ritchie, J. C., Smith, B., Walker, D. A., Gajewski, K., Wolf, V., Holmqvist, B. H., Igarashi, Y., Kremenetskii, K., Paus, A., Pisaric, M. F. J., and Vokova, V. S.: Climate change and Arctic ecosystems I. Vegetation changes north of 55°N between the last glacial maximum, mid-Holocene and present. Journal of Geophysical Research - Atmospheres, 108(D19), doi: 10.1029/2002JD002558, 2003.

Braconnot, P., Otto-Bleisner, B., Harrison, S.P., Joussaume, S., Peterschmitt, J.-Y., Abe-Ouchi, A., Crucifix, M., Driesschaert, E., Fichefet, T., Hewitt, C.D., Kagayama, M., Kitoh, A., Loutre, M.-F., Marti, O., Merkel, U., Ramstein, G., Valdes, P., Weber, L., Yu, Y., and Zhao, Y.: Results of PMIP2 coupled simulations of the mid-Holocene and Last Glacial maximum, part 1: experiments and large-scale features, Clim Past 3:261–277, 2007.

Bohner, J.: General climatic controls and topoclimatic variations in Central and High Asia, *Boreas*, 35(2), 279-295, 2006.

Bookhagen, B., Thiede, R.C., and Strecker, M.R.: Late Quaternary intensified monsoon phases control landscape evolution in the northwest Himalaya, *Geology*, 33(2), 149-152. doi: 10.1130/G20982.1, 2005.

Boos, W. R., and Kuang, Z.: Dominant control of the South Asian monsoon by orographic insulation versus plateau heating, *Nature*, 463, 218-222, 2010.

Braun, J.: A simple model for regolith formation by chemical weathering: Regolith Formation, *Journal of Geophysical Research Earth's Surface,* DOI: 10.1002/2016JF003914, 2016.

CLIMAP Project Members: Seasonal Reconstruction of the Earth's Surface at the Last Glacial Maximum. *Map and Chart Series*, Vol. 36, Geological Society of America, 18 pp., 1981.

Cohen, S.J.: Bringing the global warming issue close to home: The challenge of regional impact studies. *Bulletin of the American Meteorological Society,* 71: 520 – 526., 1990.

Delunel, R., van der Beek, P. A., Carcaillet, J., Bourlès, D. L., and Valla, P.G.: Frost-cracking control on catchment denudation rates: Insights from in situ produced 10Be concentrations in stream sediments (Ecrins–Pelvoux massif, French Western Alps), *Earth and Planetary Science Letters*, *293*(1–2), 72–83, doi:10.1016/j.epsl.2010.02.020, 2010.

Dietrich, W. E., and Perron, J.T.: The search for a topographic signature of life, *Nature*, *439*(7075), 411–418, doi:10.1038/nature04452, 2006.

Dietrich, S., Werner, M., Spangehl, T., and Lohmann, G.: Influence of orbital forcing and solar activity on water isotopes in precipitation during the mid and late Holocene, *Clim. Past*, 9, 13-26. doi:10.5194/cp-9-13-2013, 2013.

Dettman, D.L., Fang, X.M., Garzione, C.N., and Li, J.J.: Uplift-driven climate change at 12 Ma: a long delta O-18 record from the NE margin of the Tibetan plateau. *Earth and Planetary Science Letters*, 214(1-2), 267-277, 2003.

Dowsett, H.J., Robinson, M., Haywood, A., Salzmann, U., Hill, D., Sohl, L., Chandler, M., Williams, M., Foley, K., and Stoll, D.: The PRISM3D paleoenvironmental reconstruction. *Stratigraphy*, 7, 123–139, 2010.

Ehlers, T.A., and Poulsen, C.J.: Influence of Andean uplift on climate and paleoaltimetry estimates, *Earth and Planetary Science Letters*, 281(3-4), 238-248, 2009.

Etheridge, D.M., Steele, L., Langenfelds, R., Francey, R., Barnola, J., and Morgan, V.:, Natural and anthropogenic changes in atmospheric CO_2 over the last 1000 years from air in Antarctic ice and firn, *J Geophys Res* 101:4115–4128, 1996.

Etheridge, D.M., L. Steele, R. Francey, and R. Langenfelds (1998), Atmospheric methane between 1000 a.d. and present: evidence of anthropogenic emissions and climatic variability. *J Geophys Res,* 103:15979–15993

Feng, R., Poulsen, C.J., Werner, M., Chamberlain, C.P., Mix, H.T., and Mulch, A.: Early Cenozoic evolution of topography, climate, and stable isotopes in precipitation in the North American Cordillera, *American Journal of Science*, *313*(7), 613–648, 2013.

Gierz, P., Lohmann, G., and Wei, W.: Response of Atlantic Overturning to future warming in a coupled atmosphere-ocean-ice sheet model, *Geophysical Research Letters*, 42, 6811-6818, doi:10.1002/2015GL065276, 2015.

Glotzbach, C., van der Beek, P., Carcaillet, J., and Delunel, R.: Deciphering the driving forces of erosion rates on millennial to million-year timescales in glacially impacted landscapes: An example from the Western Alps, *Journal* *of Geophysical Research: Earth Surface,* 118, 1491-1515, 2013.

Gong, X., Knorr, G., Lohmann, G., and Zhang, X.: Dependence of abrupt Atlantic meridional ocean circulation changes on climate background states, *Geophysical Research Letters*, 40 (14), 3698-3704, doi:10.1002/grl.50701, 2013.

Gyssels, G., Poesen, J., Bochet, E., and Li, Y.: Impact of plant roots on the resistance of soils to erosion by water: a review, *Progress in Physical Geography*, 29, 189–217. http://doi.org/10.1191/0309133305pp443ra, 2005.

Harris, I., Jones, P.D., Osborn, T.J., and Lister, D.H.: Updated high-resolution grids of monthly climatic observations - the CRU TS3.10 Dataset, *International Journal of Climatology*, doi:10.1002/joc.3711, 2013.

Harrison, S. P., Yu, G., Takahara, H., and Prentice, I. C.: Palaeovegetation - Diversity of temperate plants in east Asia. Nature 413, 129-130, 2001.

Harrison, S.P., Bartlein, P.J., Brewer, S., Prentice, I.C., Boyd, M., Hessler, I., Holmgren, K., Izumi, K., and Willis, K.: Climate model benchmarking with glacial and mid-Holocene climates, Climate Dynamics, 43, 671-688. doi 10.1007/s00382-013-1922-6, 2013.

Haywood, A.M., Valdes, P.J., and Sellwood, B.W.: Global scale palaeoclimate reconstruction of the middle Pliocene climate using the UKMO GCM: initial results. *Global and Planetary Change,* 25 (3–4), 239–256, 2000.

Haywood, A.M., Dowsett, H.J., Otto-Bliesner, B., Chandler, M.A., Dolan, A.M., Hill, D.J., Lunt, D.J., Robinson, M.M., Rosenbloom, N., Salzmann, U., and Sohl, L.E.: Pliocene Model Intercomparison Project (PlioMIP): experimental design and boundary conditions (Experiment 1), *Geoscientific Model Development* (3), 227-242, 2010.

Haywood, A.M., Hill, D.J., Dolan, A.M., Otto-Bliesner, B., Bragg, F., Chan, W.-L., Chandler, M.A., Contoux, C., Jost, A., Kamae, Y., Lohmann, G., Lunt, D.J., Abe-Ouchi, A., Pickering, S.J., Ramstein, G., Rosenbloom, N.A., Sohl, L., Stepanek, C., Yan, Q., Ueda, H., and Zhang, Z.: Large-scale features of Pliocene climate: results from the Pliocene Model Intercomparison Project, *Clim. Past*, 9, 191-209. doi:10.5194/cp-9-191-2013, 2013.

Herman, F., Seward, D., Valla, P.G., Carter, A., Kohn, B., Willett, S.D., and Ehlers, T.A.: Worldwide acceleration of mountain erosion under a cooling climate, *Nature,* 504, 423–426. doi:10.1038/nature12877, 2013.

Hillenbrand, C.-D., and Fütterer, D.K.: Neogene to Quaternary deposition of opal on the continental rise west of the Antarctic Peninsula, ODP Leg 178, Sites 1095, 1096, and 1101. In: Barker, P.F., Camerlenghi, A., Acton, G.D., Ramsay, A.T.S. (Eds.), Proceedings of the Ocean Drilling Programme, Scientific Results, 178. Texas A and M University, College Station, Texas, pp. 1–40 (CD-ROM), 2002.

Hobley, D.E., Sinclair, H.D., and Cowie, P.A.: Processes, rates, and time scales of fluvial response in an ancient postglacial landscape of the northwest Indian Himalaya. *Geological Society of America Bulletin,* 122, 1569-1584, 2010.

Insel, N., Poulsen, C.J., and Ehlers, T.A.: Influence of the Andes Mountains on South American moisture transport, convection, and precipitation, *Climate Dynamics*, 35 (7-8), 1477-1492, 2010.

Earth Surf. Dynam. Discuss., https://doi.org/10.5194/esurf-2017-47
Manuscript under review for journal Earth Surf. Dynam.
Discussion started: 16 August 2017

Jeffery, M.L., Ehlers, T.A., Yanites, B.J., and Poulsen, C.J.: Quantifying the role of paleoclimate and Andean Plateau uplift on river incision: PALEOCLIMATE ROLE IN RIVER INCISION, *Journal of Geophysical Research: Earth Surface*, *118*(2), 852–871, doi:10.1002/jgrf.20055, 2013.

Jungclaus, J. H., Lorenz, S. J., Timmreck, C., Reick, C. H., Brovkin, V., Six, K., Segschneider, J., Giorgetta, M.A., Crowley, T.J., Pongratz, J., Krivova, N.A., Vieira, L.E., Solanski, S.K., Klocke, D., Botzet, M., Esch, M., Gayler, V., Haak, H., Raddatz, T.J., Roeckner, E., Schnur, R., Widmann, H., Claussen, M., Stevens, B., and Marotzke, J.: Climate and carbon-cycle variability over the last millennium. *Climate of the Past, 6*, 723-737. doi:10.5194/cp-6-723-2010, 2010.

Kalnay, E., Kanamitsu, M., Kistler, R., Collins, W., Deaven, D., Gandin, L., Iredell, M., Saha, S., White, G., Woollen, J., Zhu, Y., Chelliah, M., Ebisuzaki, W., Higgins, W., Janowiak, J., Mo, K.C., Ropelewski, C., Wang, J., Leetmaa, A., Reynolds, R., Jenne, R., and Joseph, D.: The NCEP/NCAR 40-year reanalysis project. *Bulletin of the American Meteorological Society*, 77(3), 437-471, 1996.

Kistler, R., Collins, W., Saha, S., White, G., Woollen, J., Kalnay, E., Chelliah, M., Ebisuzaki, W., Kanamitsu, M., Kousky, V., Van den Dool, H., Jenne, R., and Fiorino, M.: The NCEP−NCAR 50−Year Reanalysis: Monthly Means CD−ROM and Documentation. *Bulletin of the American Meteorological Society*, 82(2), 247–267, 2001.

Kirchner, J.W., Finkel, R.C., Riebe, C.S., Granger, D.E., Clayton, J.L., King, J.G., and Megahan, W.F.: Mountain erosion over 10 yr, 10 k.y., and 10 m.y. time scales, *Geology,* 29 (7), 591-594, 2001.

Knorr, G., Butzin, M., Micheels, A., and Lohmann, G.: A Warm Miocene Climate at Low Atmospheric CO2 levels. Geophysical Research Letters, 38, L20701, doi:10.1029/2011GL048873, 2011.

Koons, P.O., Zeitler, P.K., and Hallet, B.: 5.14 Tectonic Aneurysms and Mountain Building, in *Treatise on Geomorphology*, pp. 318–349, Elsevier, 2013.

Kraus, H.: Die Atmosphäre der Erde. Eine Einführung in die Meteorologie. Berlin, 2001.

Kutzbach, J.E., Guetter, P.J., Ruddiman, W.F., and Prell, W.L.: Sensitivity of Climate to Late Cenozoic Uplift in Southern Asia and the American West - Numerical Experiments, *Journal of Geophysical Research-Atmospheres*, 94(D15), 18393-18407, 1989.

Kutzbach, J.E., Prell, W.L., and Ruddiman, W.F.: Sensitivity of Eurasian Climate to Surface Uplift of the Tibetan Plateau, *Journal of Geology*, 101(2), 177-190, 1993.

Lease, R.O., and Ehlers, T.A.: Incision into the Eastern Andean Plateau During Pliocene Cooling, *Science*, *341*(6147), 774–776, doi:10.1126/science.1239132, 2013.

Legates, D.R., and Willmott, C.J.: Mean Seasonal and Spatial Variability in Gauge-Corrected, Global Precipitation, *International Journal of Climatology 10(2), 111-127. doi: 10.1002/joc.3370100202,* 1990.

Li, J., Ehlers, T.A., Werner, M., Mutz, S.G., Steger, C., Paeth, H.: Late quarternary climate, precipitation $\delta^{18}O$, and Indian monsoon variations over the Tibetan Plateau. *Earth and Planetary Science Letters* 457, 412-422, 2017.

Lohmann, G., Pfeiffer, M., Laepple, T., Leduc, G., and Kim, J.-H.: A model-data comparison of the Holocene global sea surface temperature evolution. Clim. Past, 9, 1807-1839, doi:10.5194/cp-9-1807-2013, 2013.

Lorenz, S.J., and Lohmann, G.: Acceleration technique for Milankovitch type forcing in a coupled atmosphere-ocean circulation model: method and application for the Holocene. Climate Dynamics (2004) 23: 727. doi:10.1007/s00382-004-0469-y, 2004.

Marshall, J.A., Roering, J.J., Bartlein, P.J., Gavin, D.G., Granger, D.E., Rempel, A.W., Praskievicz, S.J., and Hales, T.C.: Frost for the trees: Did climate increase erosion in unglaciated landscapes during the late Pleistocene? *Science Advances*, 1, 1-10, 2015.

Marston, R.A.: Geomorphology and vegetation on hillslopes: Interactions, dependencies, and feedback loops, *Geomorphology*, 116(3–4), 206–217. doi:http://doi.org/10.1016/j.geomorph.2009.09.028, 2010.

Matsuoka, N., and Murton, J.: Frost weathering: Recent advances and future directions. *Permafr. Periglac. Process.* 19, 195–210, 2008.

Matsuoka, N.: Solifluction rates, processes and landforms: A global review. *Earth Science Reviews* 55, 107–134, 2001.

Maussion, F., Scherer, D., Mölg, T., Collier, E., Curio, J., and Finkelnburg, R.: Precipitation seasonality and variability over the Tibetan Plateau as resolved by the High Asia Reanalysis, *J. Climate, 27, 1910-1927, doi:10.1175/JCLI-D-13-00282.1*, 2014

Mesinger, F., DiMego, G., Kalnay, E., Mitchell, K., Shafran, P.C., Ebisuzaki, W., Jovic, D., Woollen, J., Rogers, E., Berbery, E.H., Ek, M.B., Fan, Y., Grumbine, R., Higgins, W., Li, H., Lin, Y., Manikin, G., Parrish, D., and Shi, W.:

North American Regional Reanalysis, *Bulletin of the American Meteorological Society, 87, 343–360.doi:10.1175/BAMS-87-3-343, 2006.*

Molnar, P., Boos, W.R., and Battisti, D.S.: Orographic Controls on Climate and Paleoclimate of Asia: Thermal and Mechanical Roles for the Tibetan Plateau, *Annual Review of Earth and Planetary Sciences*, 38, 77-102, 2010.

Molnar, P., and England, P.: Late Cenozoic uplift of mountain ranges and global climate change: chicken or egg?, *Nature*, 346, 29-34, 1990.

Montgomery, D.R.: Slope distributions, threshold hillslopes, and steady-state topography, *American Journal of Science,* 301, 432-454, 2001.

Montgomery, D.R., Balco, G., and Willett, S.D.: Climate, tectonics, and the morphology of the Andes, *Geology*, 29(7), 579-582, 2001.

Moon, S., Chamberlain, C.P., Blisniuk, K., Levine, N., Rood, D.H., Hilley, G.E.: Climatic control of denudation in the deglaciated landscape of the Washington Cascades, *Nature Geoscience,* 4, 469-473, 2011.

Moulton, K.L., and Berner, R.A.: Quantification of the effect of plants on weathering: studies in Iceland, *Geology*, 26, 895-898, 1998.

Earth Surf. Dynam. Discuss., https://doi.org/10.5194/esurf-2017-47
Manuscript under review for journal Earth Surf. Dynam.
Discussion started: 16 August 2017

Mutz, S.G., Ehlers, T.A., Li, J., Steger, C., Peath, H., Werner, M., Poulsen, C.J.: Precipitation $\delta^{18}O$ over the South Asia Orogen from ECHAM5-wiso Simulation: Statistical Analysis of Temperature, Topography and Precipitation. *Journal of Geophysical Research-Atmospheres*, 121(16),9278-9300, doi: 10.1002/2016JD024856, 2016.

Otto-Bliesner, B.L., Brady, C.B., Clauzet, G., Tomas, R., Levis, S., and Kothavala, Z.: Last Glacial Maximum and Holocene Climate in CCSM3. Journal of Climate, 19, 2526-2544, 2006.

Paeth, H.: Key Factors in African Climate Change Evaluated by a Regional Climate Model, *Erdkunde*, 58, 290-315, 2004.

Pfeiffer, M., and Lohmann, G.: Greenland Ice Sheet influence on Last Interglacial climate: global sensitivity studies performed with an atmosphere-ocean general circulation model. *Climate of the Past*, 12, pp. 1313-1338, doi:10.5194/cp-12-1313-2016, 2016.

Pickett, E.J., Harrison, S.P., Flenley, J., Grindrod, J., Haberle, S., Hassell, C., Kenyon, C., MacPhail, M., Martin, H., Martin, A.H., McKenzie, M., Newsome, J.C., Penny, D., Powell, J., Raine, J.I., Southern, W., Stevenson, J., Sutra, J.-P., Thomas, I., van der Kaars, S., Ward, J.: Pollen-based reconstructions of biome distributions for Australia, South-East Asia and the Pacific (SEAPAC region) at 0, 6000 and 18,000 14C years B.P.. Journal of Biogeography, 31, 1381–1444, doi: 10.1111/j.1365-2699.2004.01001.x, 2004.

Prentice, I. C., Jolly, D., and BIOME 6000 Participants. (2000). Mid-Holocene and glacial-maximum vegetation geography of the northern continents and Africa. Journal of Biogeography 27, 507-519.

Raymo, M.E., and Ruddiman, W.F.: Tectonic forcing of late cenozoic climate. *Nature*, 359(6391), 117-122, 1992.

Robinson, M.M.: New quantitative evidence of extreme warmth in the Pliocene Arctic, Stratigraphy 6, 265–275, 2009.

Roeckner, E., Bäuml, G., Bonaventura, L., Brokoph, R., Esch, M., Giorgetta, M., Hagemann, S., Kirchner, I., Kornblueh, L., Manzini, E., Rhodin, A., Schlese, U., Schulzweida, U., and Tompkins, A.: The atmospheric general circulation model ECHAM5. Part I: Model description. Rep. 349Rep., 127 pp, Max Planck Institute for Meteorology, Hamburg, 2003.

Roering, J.J., Marshall, J., Booth, A.M., Mort, M., and Jin, Q.: Evidence for biotic controls on topography and soil production, *Earth and Planetary Science Letters*, *298*(1–2), 183–190, doi:10.1016/j.epsl.2010.07.040, 2010.

Salzmann, U., Williams, M., Haywood, A.M., Johnson, A.L.A., Kender, S., and Zalasiewicz, J.: Climate and environment of a Pliocene warm world. *Palaeogeography, Palaeoclimatology, Palaeoecology*, 309 (1-8), 2011.

Sarnthein, M., Gersonde, R., Niebler, S., Pflaumann, U., Spielhagen, R., Thiede, J., Wefer, G., Weinelt, M.: Overview of Glacial Atlantic Ocean Mapping (GLAMAP 2000), *Paleoceanography*, 18(2), doi:10.1029/2002PA000769, 2003.

Schäfer-Neth C., and Paul, A.: The Atlantic Ocean at the last glacial maximum: objective mapping of the GLAMAP sea-surface conditions. In: Wefer G, Mulitza S, Ratmeyer V (eds) The South Atlantic in the late quaternary: reconstruction of material budgets and current systems. Springer, Berlin, pp 531–548, 2003.

Schaller, M., von Blanckenburg, F., Veldkamp, A., Tebbens, L.A., Hovius, N., and Kubik, P.W.: A 30 000 yr record of erosion rates from cosmogenic 10 Be in Middle European river terraces, *Earth and Planetary Science Letters*, *204*(1), 307–320, 2002.

Schaller, M., and Ehlers T.A.: Limits to quantifying climate driven changes in denudation rates with cosmogenic radionuclides, *Earth and Planetary Science Letters*, v. 248, pp. 153-167. doi:10.1016/j.epsl.2006.05.027, 2006.

Simmons, A.J., Burridge, D.M., Jarraud, M., Girard, C., and Wergen, W.: The ECMWF Medium-Range prediction models development of the numerical formulations and the impact of increased resolution, Meteorology and Atmospheric Physics, 40(1-3), 28-60, 1989.

Sohl, L.E., Chandler, M.A., Schmunk, R.B., Mankoff, K., Jonas, J.A., Foley, K.M., and Dowsett, H.J.: PRISM3/GISS topographic reconstruction, *U.S. Geological Survey Data Series,* 419, 6p., 2009.

Sowers T., Alley, R.B., and Jubenville, J.: Ice core records of atmospheric N_2O covering the last 106,000 years. *Science*, 301:945–948, 2003.

Stepanek, C., and Lohmann, G.: Modelling mid-Pliocene climate with COSMOS , *Geosci. Model Dev.* , 5 , pp. 1221-1243 . doi:10.5194/gmd-5-1221-2012, 2012.

Takahashi, K., and Battisti, D.: Processes controlling the mean tropical pacific precipitation pattern. Part I: The Andes and the eastern Pacific ITCZ. *Journal of Climate*, 20(14), 3434-3451, 2007a.

Takahashi, K., and Battisti, D.: Processes controlling the mean tropical pacific precipitation pattern. Part II: The SPCZ and the southeast pacific dry zone. Journal of Climate, 20(23), 5696-5706, 2007b.

Thiede, R.C., and Ehlers, T.A.: Large spatial and temporal variations in Himalayan denudation. *Earth and Planetary Science Letters*, *374*, *256-257. doi:10.1016/j.epsl.2013.03.004*, 2013.

Thomas, A.: The climate of the Gongga Shan range, Sichuan Province, PR China. Arctic and Alpine Research, 29(2), 226-232, 1997.

Uppala, S.M., Kållberg, P.W., Simmons, A.J., Andrae, U., da Costa Bechtold, V., Fiorino, M., Gibson, J.K., Haseler, J., Hernandez, A., Kelly, G.A., Li, X., Onogi, K., Saarinen, S., Sokka, N., Allan, R.P., Andersson, E., Arpe, K., Balmaseda, M.A., Beljaars, A.C.M., van de Berg, L., Bidlot, J., Bormann, N., Caires, S., Chevallier, F., Dethof, A., Dragosavac, M., Fisher, M. Fuentes, M., Hagemann, S., Hólm, E., Hoskins, B.J., Isaksen, L., Janssen, P.A.E.M., Jenne, R., McNally, A.P., Mahfouf, J.-F., Morcrette, J.-J , Rayner, N.A., Saunders, R.W., Simon, P., Sterl, A., Trenberth, K.E., Untch, A., Vasiljevic, D., Viterbo, P., and Woollen, J.: The ERA-40 re-analysis. Quart. *J. R. Meteorol. Soc.*, 131, 2961-3012, 2005.

von Blanckenburg, F., Bouchez, J., Ibarra, D.E., and Maher, K.: Stable runoff and weathering fluxes into the oceans over Quaternary climate cycles, *Nature Geoscience*, *8*(7), 538–542, doi:10.1038/ngeo2452, 2015.

Valla, P.G., Shuster, D.L., and van der Beek, P.A.: Significance increase in relief of European Alps during mid-Pleistocene glaciations. *Nature Geoscience*, 4, 688–692. doi:10.1038/ngeo1242, 2011.

Wei, W., and Lohmann, G.: Simulated Atlantic Multidecadal Oscillation during the Holocene. *Journal of Climate*, 25, 6989–7002. doi: http://dx.doi.org/10.1175/JCLI-D-11-00667.1, 2012.

Whipple, K.X, Kirby, E., and Broecklehurst, S.H.: Geomorphic limits to climate-induced increases in topographic relief. *Nature*, 401, 39-43. doi:10.1038/43375, 1999.

Whipple, K.X., and Tucker, G.E.: Dynamics of the stream-power river incision model: Implications for height limits of mountain ranges, landscape response timescales, and research needs, *Journal of Geophysical Research-Solid Earth,* 104, 17661-17674, 1999.

Whipple, K. X.: The influence of climate on the tectonic evolution of mountain belts, *Nat. Geosci.*, 2, doi:10.1038/ngeo413, 2009.

Wilks, D.S.: Statistical methods in the atmospheric sciences - 3rd ed. Academic Press, Oxford, 2011.

Willett, S.D., Schlunegger, F., and Picotti, V.: Messinian climate change and erosional destruction of the central European Alps. *Geology*, 34(8), 613-616, 2006.

Wilson, G.S., Barron, J.A., Ashworth, A.C., Askin, R.A., Carter, J.A., Curren, M.G., Dalhuisen, D.H., Friedmann, E.I., Fyodorov-Davidov, D.G., Gilichinsky, D.A., Harper, M.A., Harwood, D.M., Hiemstra, J.F., Janecek, T.R., Licht, K.J., Ostroumov, V.E., Powell, R.D., Rivkina, E.M., Rose, S.A., Stroeven, A.P., Stroeven, P., van der Meer, J.J.M., Wizevich, M.C.: The Mount Feather Diamicton of the Sirius Group: an accumulation of indicators of Neogene Antarctic glacial and climatic history, *Palaeogeography, Palaeoclimatology, Palaeoecology,* 182 (1–2), 117–131, 2002.

Yanites, B.J., and Ehlers, T.A.: Global climate and tectonic controls on the denudation of glaciated mountains. *Earth and Planetary Science Letters,* 325, 63-75, 2012.

Zhang, X., Lohmann, G., Knorr, G., and Xu X.: Different ocean states and transient characteristics in Last Glacial Maximum simulations and implications for deglaciation. *Clim. Past*, 9, 2319-2333, doi:10.5194/cp-9-2319-2013, 2013a.

Zhang, R., Yan, Q., Zhang, Z.S., Jiang, D., Otto-Bliesner, B.L., Haywood, A.M., Hill, D.J., Dolan, A.M., Stepanek, C., Lohmann, G., Contoux, C., Bragg, F., Chan, W.-L., Chandler, M.A., Jost, A., Kamae, Y., Abe-Ouchi, A., Ramstein, G., Rosenbloom, N.A., Sohl, L., and Ueda, H.: East Asian monsoon climate simulated in the PlioMIP. Clim. Past, 9, 2085-2099, doi:10.5194/cp-9-2085-2013, 2013b.

Zhang, X., Lohmann, G., Knorr, G., and Purcell C.: Abrupt glacial climate shifts controlled by ice sheet changes. *Nature*, 512 (7514), 290-294, doi:10.1038/nature13592, 2014.

Zhisheng, A., Kutzbach, J.E., Prell, W.L., and Porter, S.C.: Evolution of Asian monsoons and phased uplift of the South Asiaan plateau since Late Miocene times. *Nature*, 411(6833), 62-66, 2001.

Earth Surf. Dynam. Discuss., https://doi.org/10.5194/esurf-2017-47
Manuscript under review for journal Earth Surf. Dynam.
Discussion started: 16 August 2017

Figures

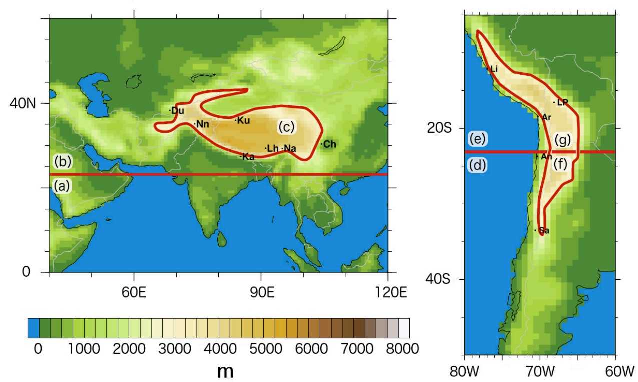

Figure 1

Earth Surf. Dynam. Discuss., https://doi.org/10.5194/esurf-2017-47
Manuscript under review for journal Earth Surf. Dynam.
Discussion started: 16 August 2017

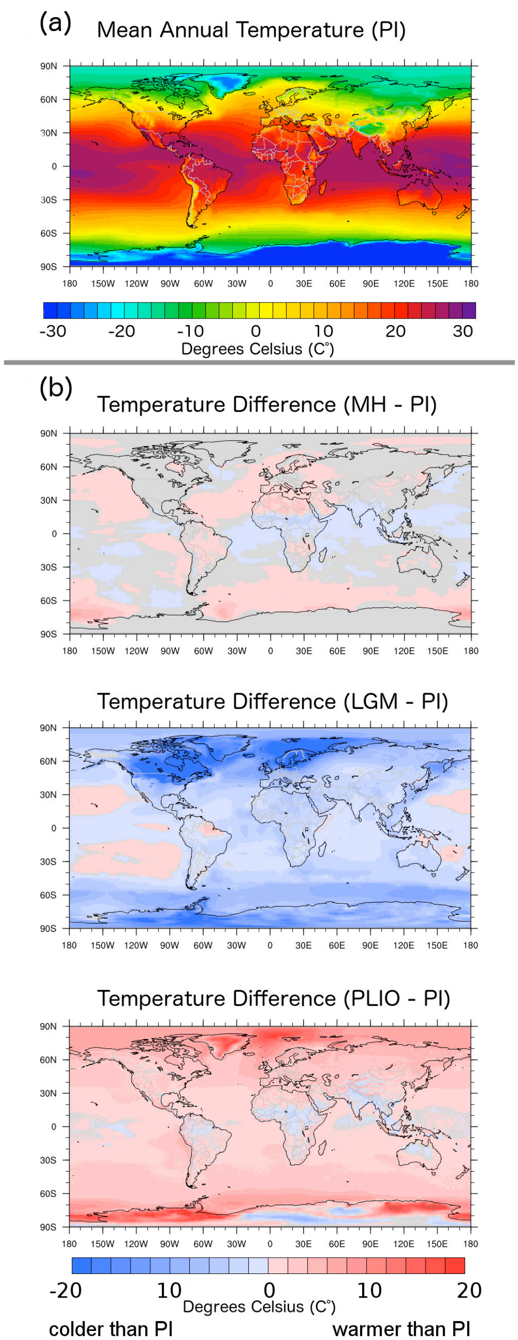

Figure 2

Earth Surf. Dynam. Discuss., https://doi.org/10.5194/esurf-2017-47
Manuscript under review for journal Earth Surf. Dynam.
Discussion started: 16 August 2017

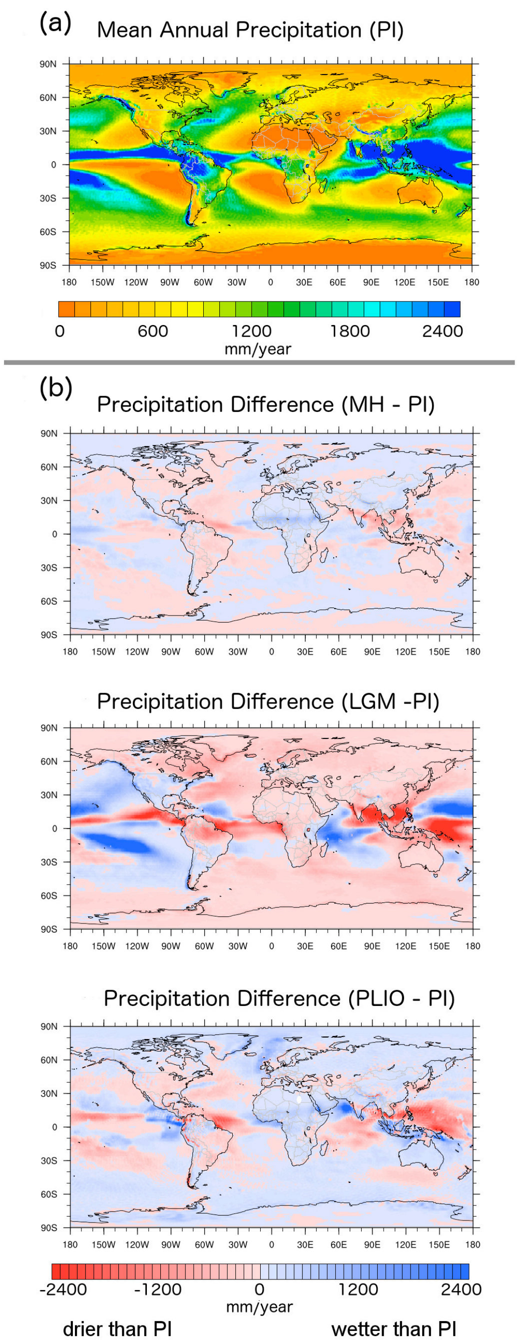

Figure 3

Earth Surf. Dynam. Discuss., https://doi.org/10.5194/esurf-2017-47
Manuscript under review for journal Earth Surf. Dynam.
Discussion started: 16 August 2017

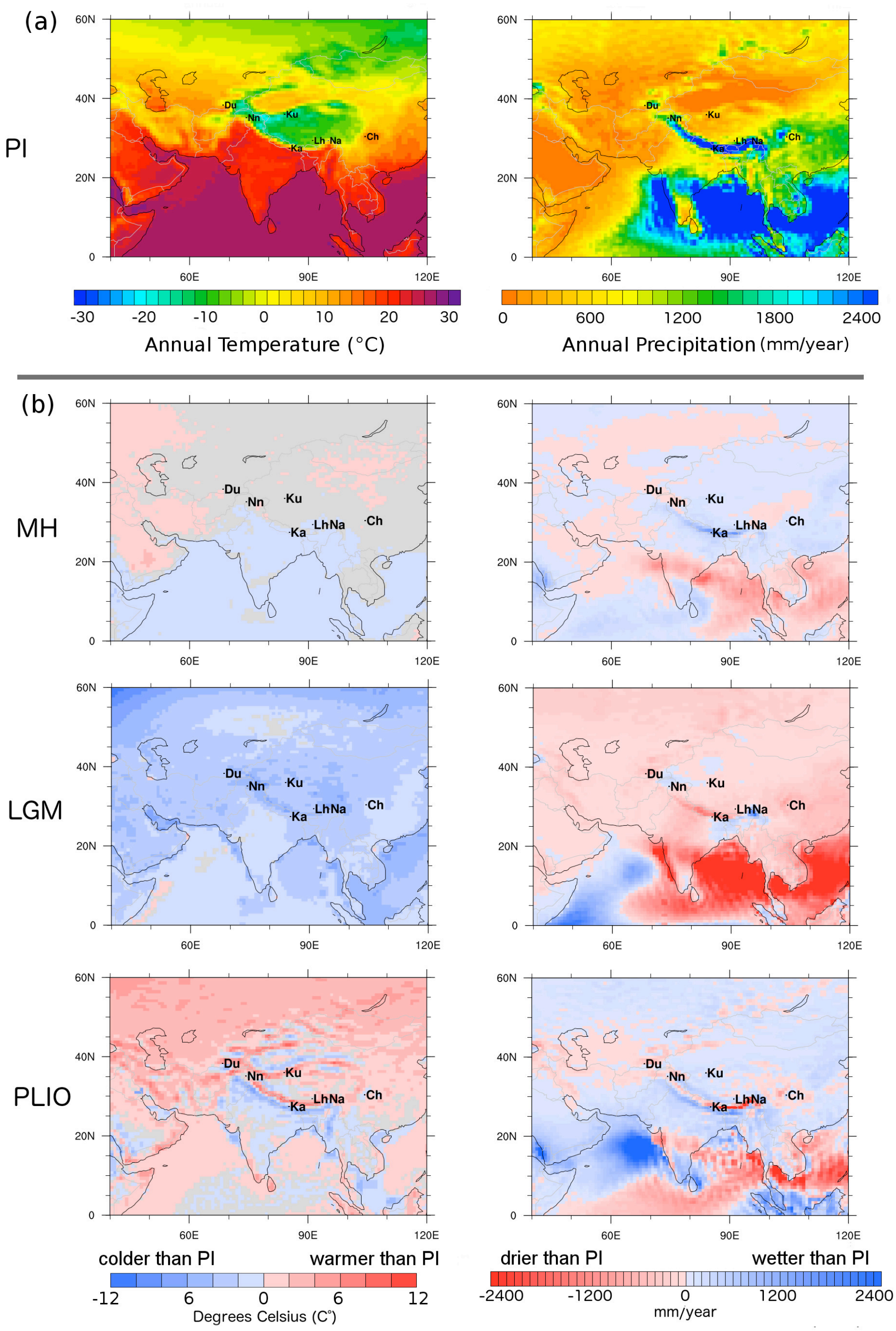

Figure 4

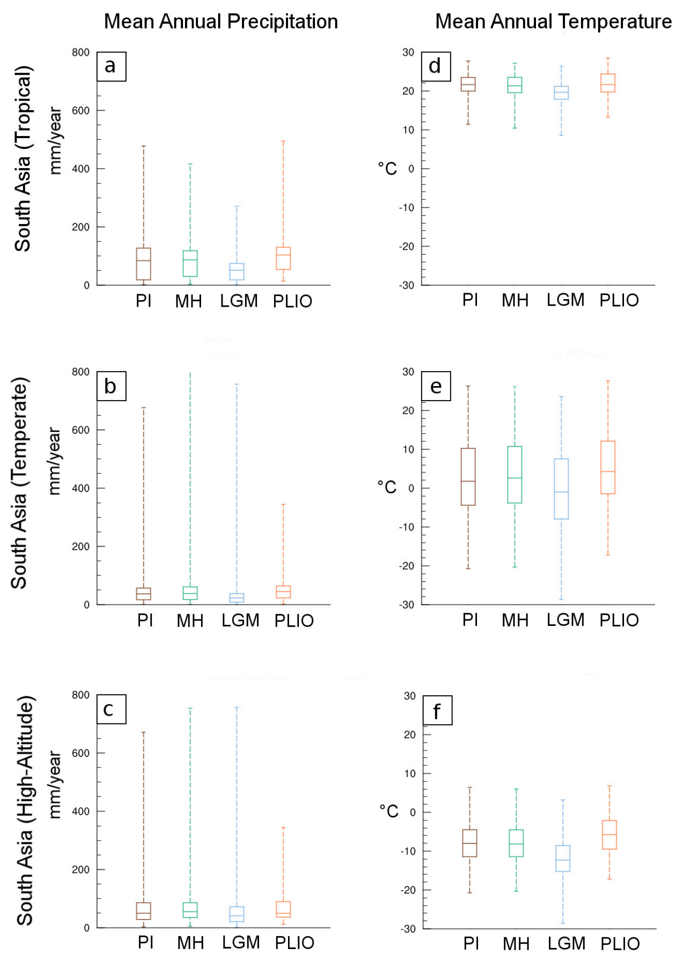
Mean Annual Precipitation
Mean Annual Temperature
South Asia (Tropical)
South Asia (Temperate)
South Asia (High-Altitude)
mm/year
°C
a
b
c
d
e
f
PI
MH
LGM
PLIO

Figure 5

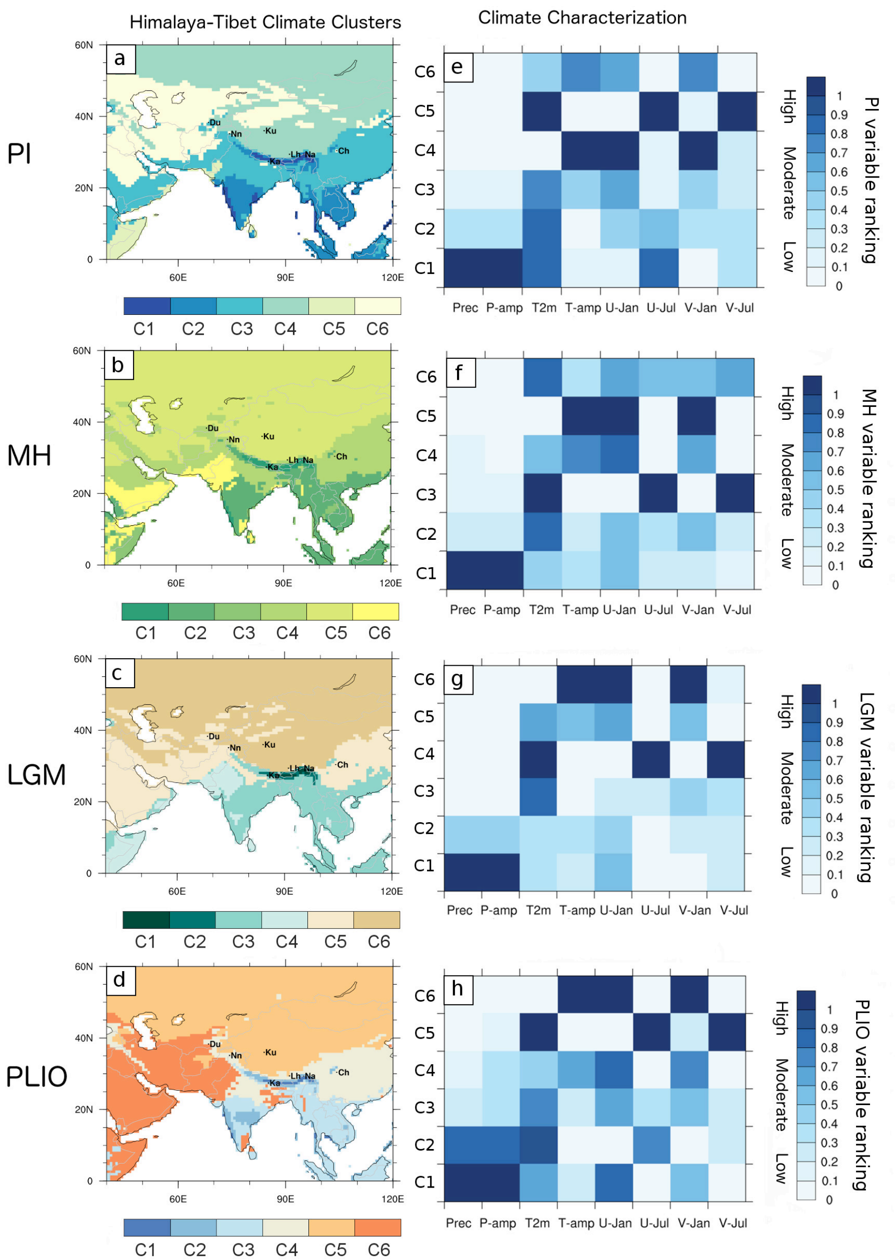
Himalaya-Tibet Climate Clusters
Climate Characterization
PI
MH
LGM
PLIO
a
b
c
d
e
f
g
h
C1 C2 C3 C4 C5 C6
Prec P-amp T2m T-amp U-Jan U-Jul V-Jan V-Jul
High Moderate Low
PI variable ranking
MH variable ranking
LGM variable ranking
PLIO variable ranking
60N 40N 20N 0
60E 90E 120E
Du Nn Ku Lh Na Ka Ch
0 0.1 0.2 0.3 0.4 0.5 0.6 0.7 0.8 0.9 1

Figure 6

Earth Surf. Dynam. Discuss., https://doi.org/10.5194/esurf-2017-47
Manuscript under review for journal Earth Surf. Dynam.
Discussion started: 16 August 2017

Earth Surface Dynamics
Discussions
Open Access

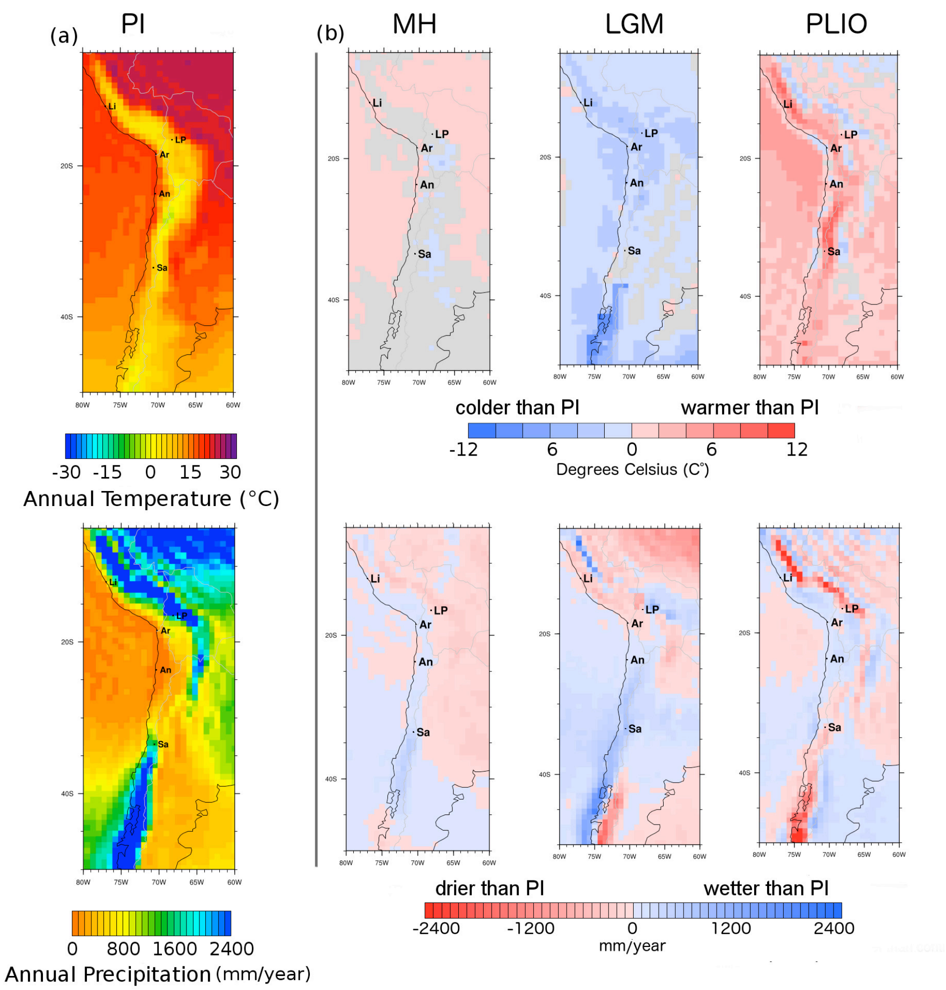

Figure 7

Earth Surf. Dynam. Discuss., https://doi.org/10.5194/esurf-2017-47
Manuscript under review for journal Earth Surf. Dynam.
Discussion started: 16 August 2017

927

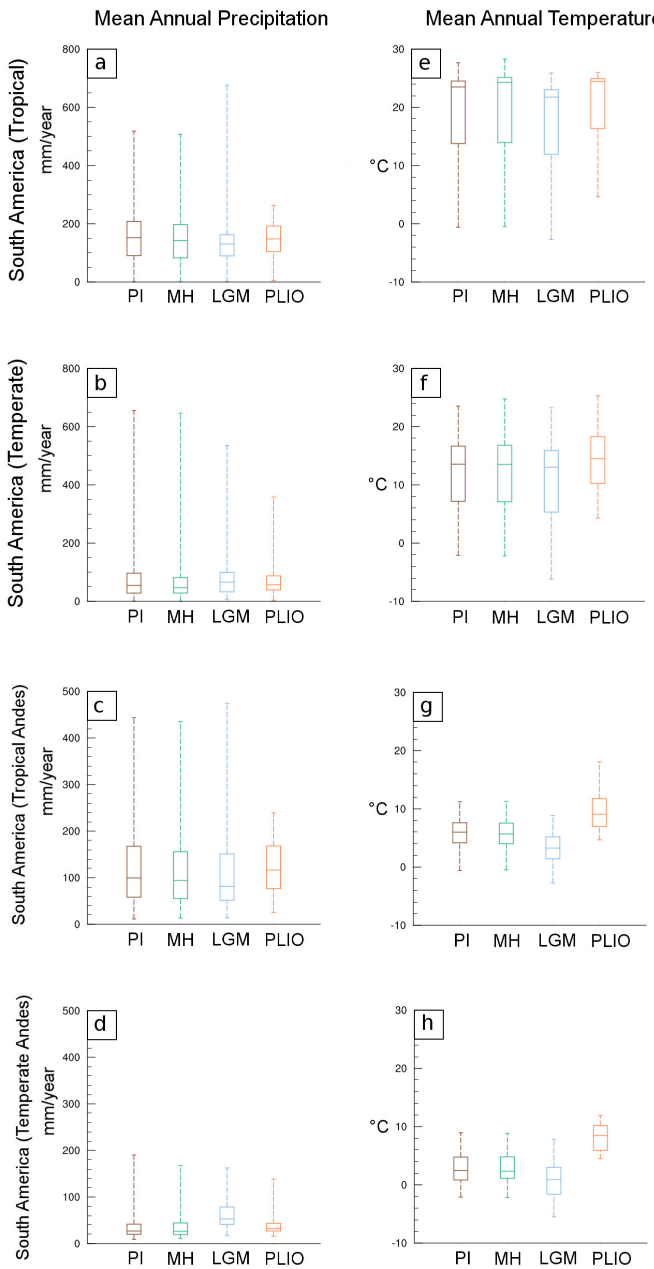

928

929 Figure 8

930

Earth Surf. Dynam. Discuss., https://doi.org/10.5194/esurf-2017-47
Manuscript under review for journal Earth Surf. Dynam.
Discussion started: 16 August 2017

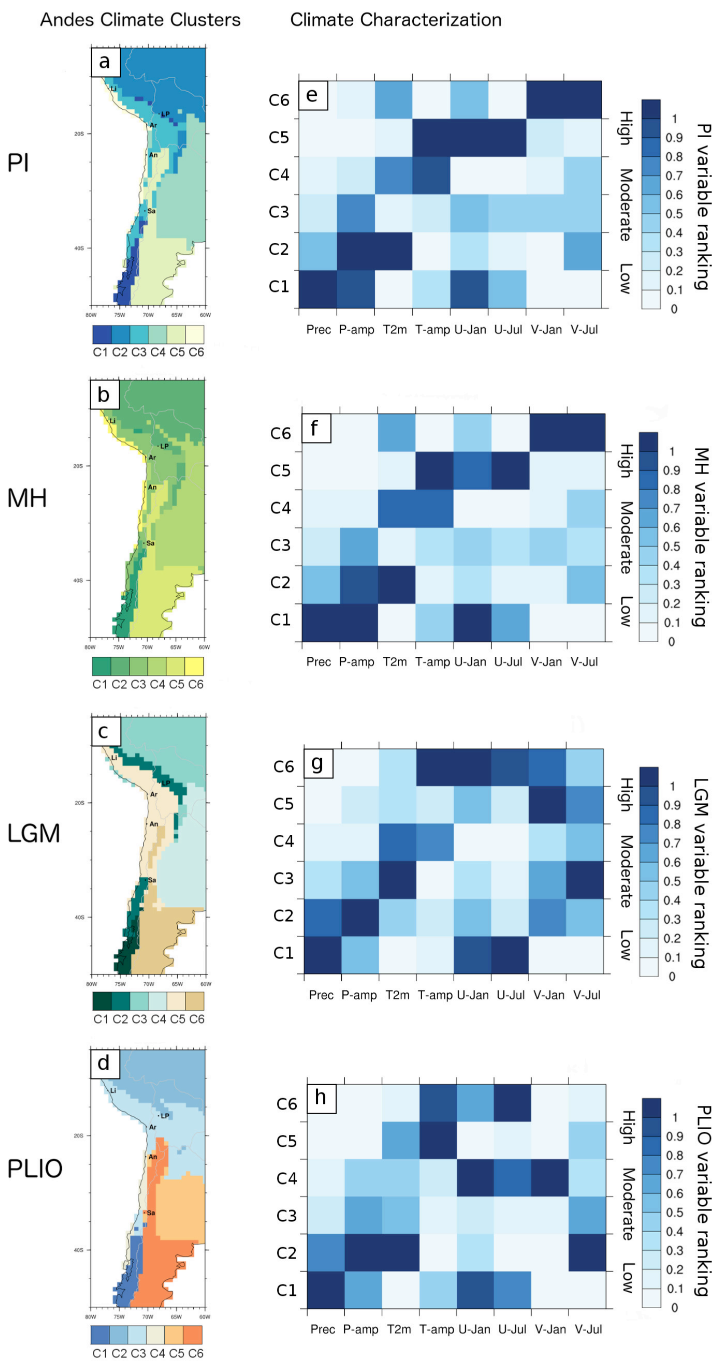

Figure 9

Earth Surf. Dynam. Discuss., https://doi.org/10.5194/esurf-2017-47
Manuscript under review for journal Earth Surf. Dynam.
Discussion started: 16 August 2017

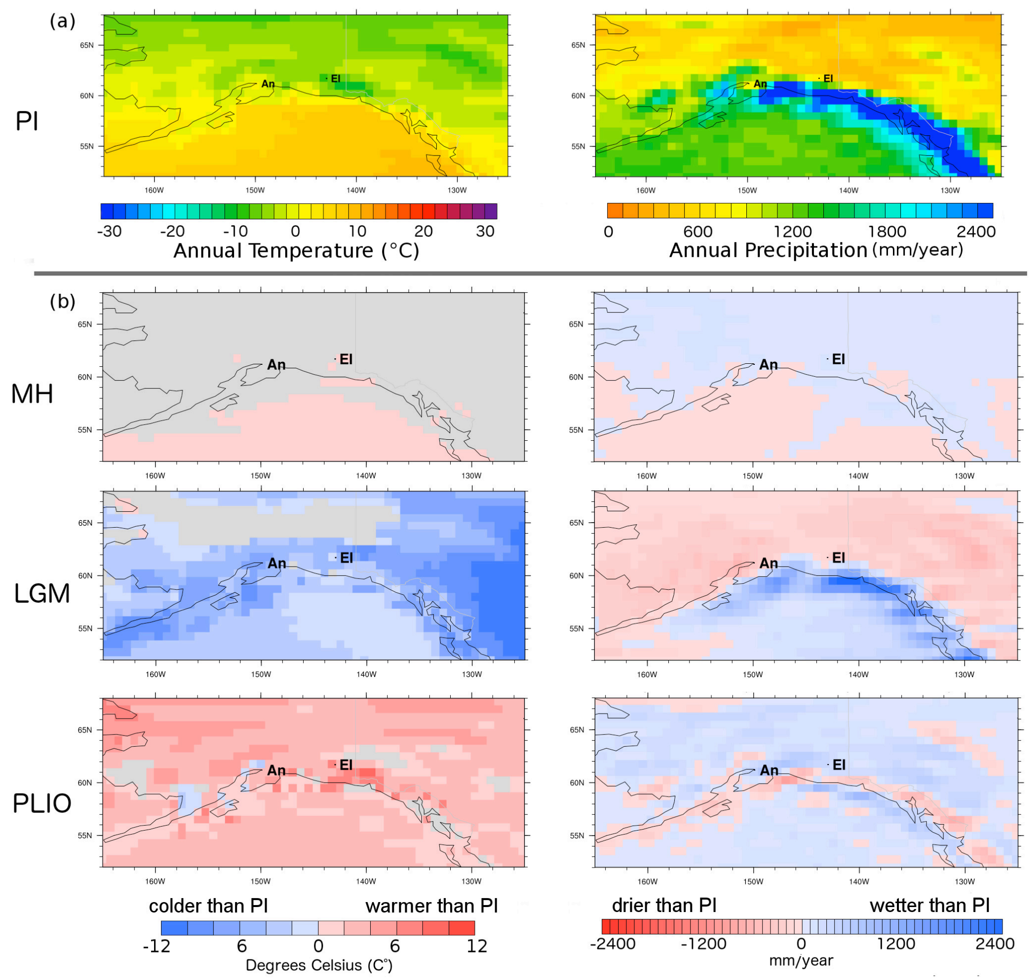

Figure 10

Earth Surf. Dynam. Discuss., https://doi.org/10.5194/esurf-2017-47
Manuscript under review for journal Earth Surf. Dynam.
Discussion started: 16 August 2017

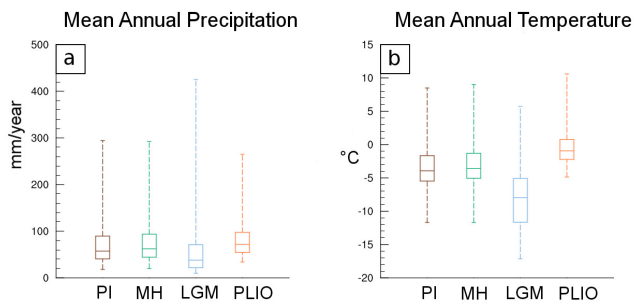

Figure 11

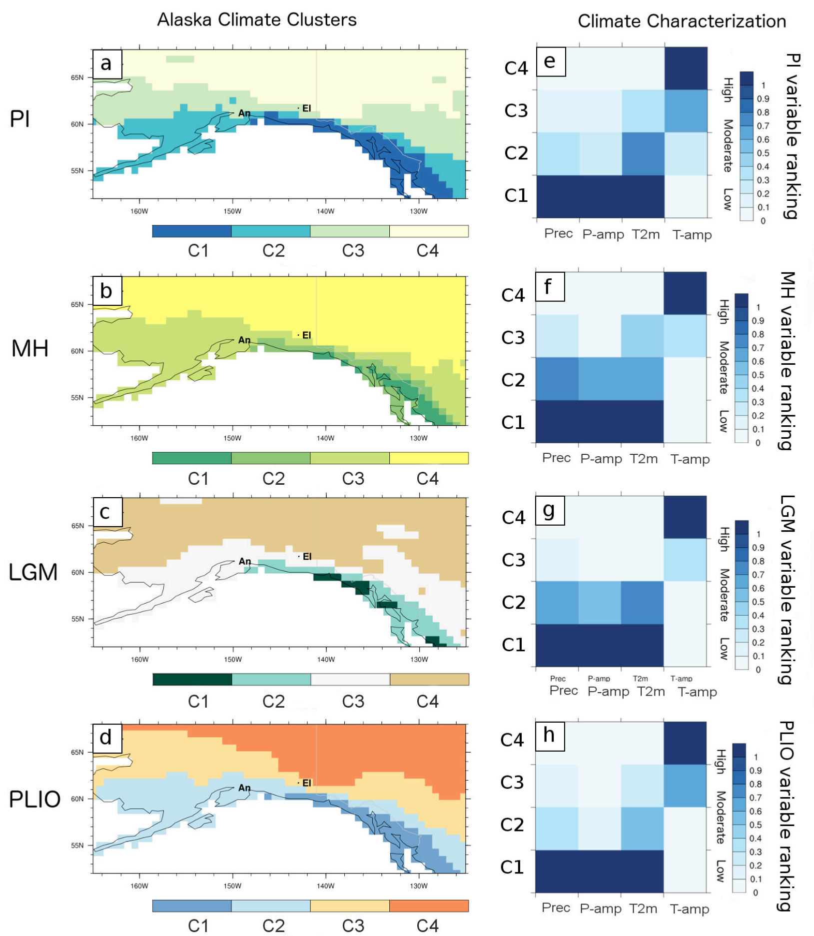

Figure 12

Earth Surf. Dynam. Discuss., https://doi.org/10.5194/esurf-2017-47
Manuscript under review for journal Earth Surf. Dynam.
Discussion started: 16 August 2017

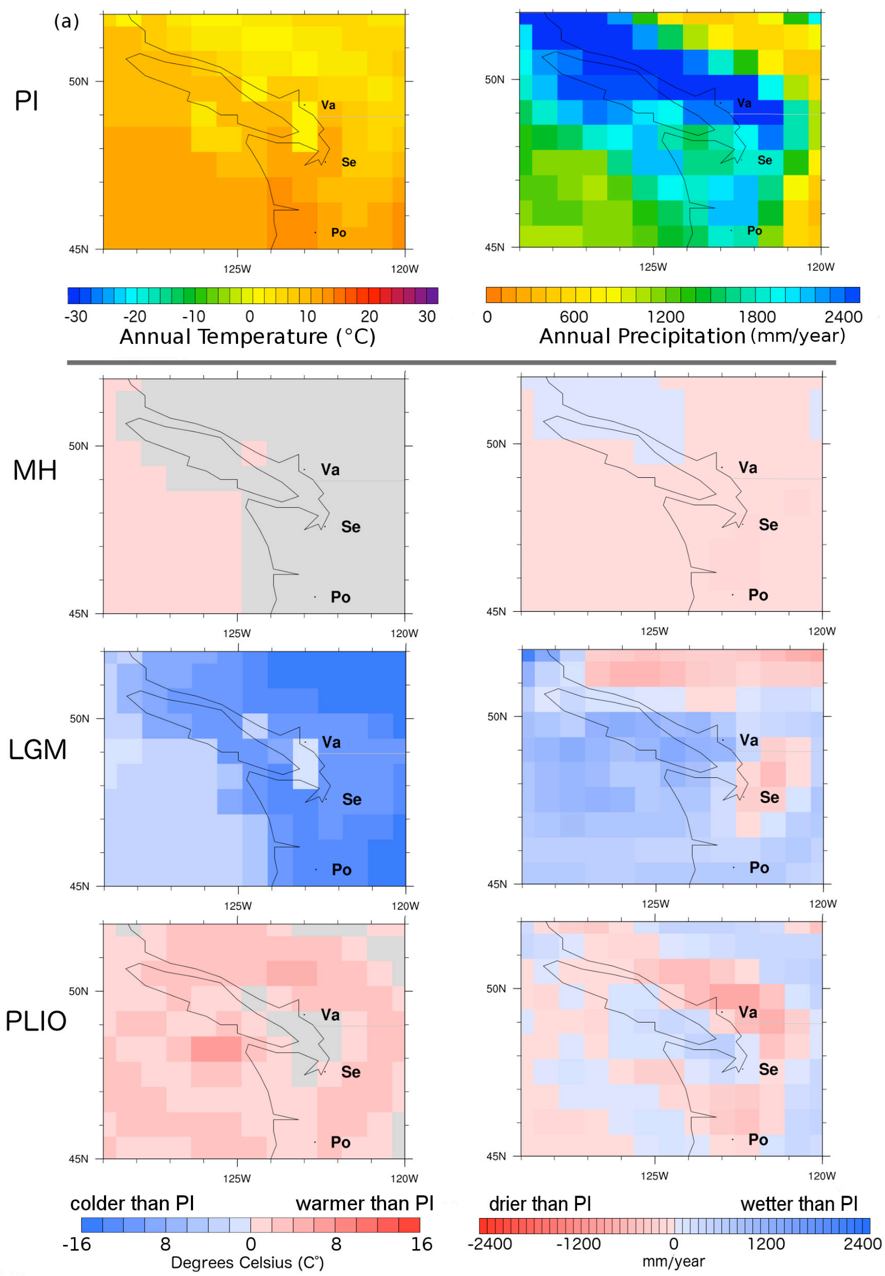

Figure 13

Earth Surf. Dynam. Discuss., https://doi.org/10.5194/esurf-2017-47
Manuscript under review for journal Earth Surf. Dynam.
Discussion started: 16 August 2017

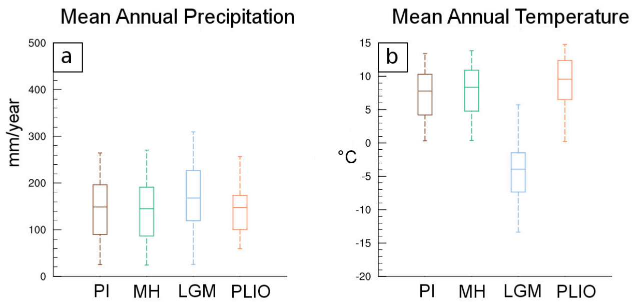

953

954 Figure 14

Earth Surf. Dynam. Discuss., https://doi.org/10.5194/esurf-2017-47
Manuscript under review for journal Earth Surf. Dynam.
Discussion started: 16 August 2017

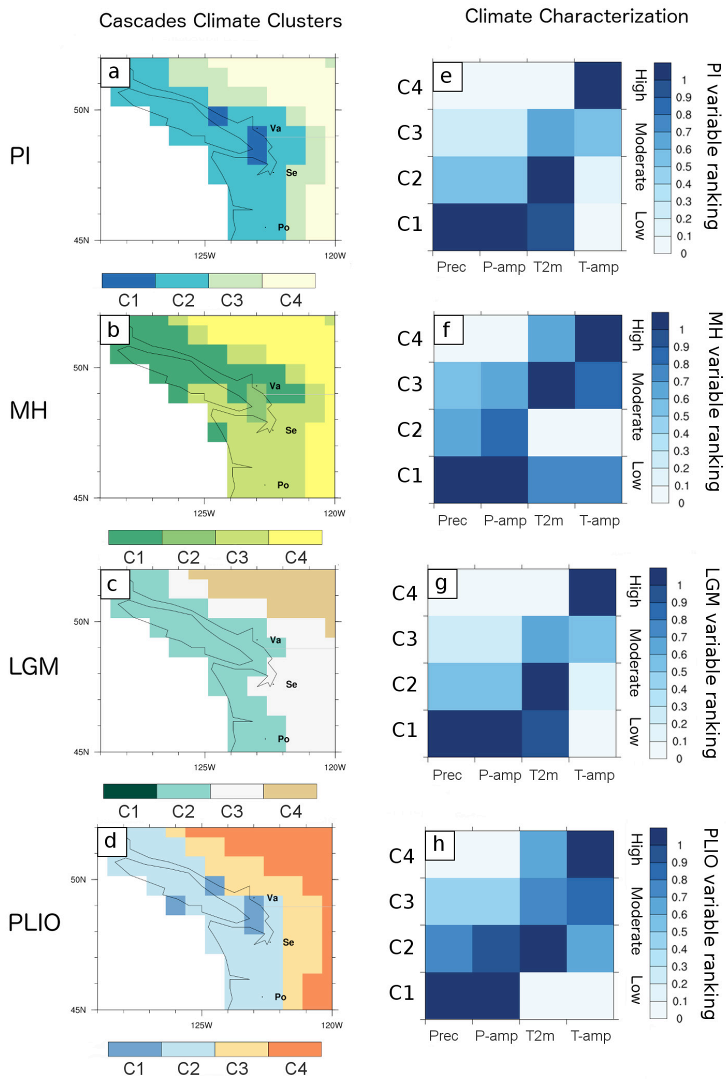

955

956 Figure 15